SIAM/ASA J. Uncertainty Quantification
Vol. 13, No. 2, pp. 518–542

An Inverse Source Problem for the Stochastic Multiterm Time-Fractional Diffusion-Wave Equation*

Xiaoli Feng†, Qiang Yao†, Peijun Li‡, and Xu Wang§

Abstract. This paper concerns both the direct and inverse source problems for the stochastic multiterm time-fractional diffusion-wave equation driven by a fractional Brownian motion. Regarding the direct problem, the well-posedness is established and the regularity of the solution is characterized for the equation. In the inverse problem, the uniqueness and instability are investigated on the determination of the diffusion coefficient in the random source. Furthermore, a reconstruction formula is provided for the phaseless Fourier modes of the diffusion coefficient in the random source, based on the variance of the boundary data. To reconstruct the time-dependent source function from its phaseless Fourier modes, the PhaseLift algorithm, combined with a spectral cut-off regularization technique, is employed to tackle the phase retrieval problem. The effectiveness of the proposed method is demonstrated through numerical experiments.

Key words. inverse random source problem, multiterm time-fractional diffusion-wave equation, fractional Brownian motion, mild solution, uniqueness, instability

MSC codes. 35R30, 35R11, 60H15

DOI. 10.1137/23M1628334

1. Introduction.

Time-fractional differential equations (TFDEs) have a wide range of applications across diverse fields, including mathematics, physics, engineering, biology, and finance. They offer valuable tools for modeling complex phenomena characterized by memory effects, nonlocal behaviors, and anomalous diffusion processes. A multitude of instances of mathematical analyses, numerical studies, and practical applications of TFDEs can be found in references such as [14, 28, 34, 36] and their associated citations. In certain applications, it has been observed that the order of fractional derivatives in some models can vary within the range of $(0, 2)$, as demonstrated in studies such as [5, 6]. To address these scenarios, researchers have introduced the concept of distributed order TFDEs. A special case of the distributed

*Received by the editors January 2, 2024; accepted for publication (in revised form) January 16, 2025; published electronically April 23, 2025.
https://doi.org/10.1137/23M1628334
Funding: The work of the first and second authors was supported by the Natural Science Basic Research Program of Shaanxi (2024JC-YBMS-034). The work of the third author was supported by the National Key R&D Program of China (2024YFA1012300). The work of the fourth author was supported by NNSF of China (11971470, 11871068, and 12288201), by the National Key R&D Program of China (2024YFA1012300 and 2024YFA1015900), and by the CAS Project for Young Scientists in Basic Research (YSBR-087).

†School of Mathematics and Statistics, Xidian University, Xi'an 713200, China (xiaolifeng@xidian.edu.cn, yqiang@stu.xidian.edu.cn).
‡State Key Laboratory of Mathematical Sciences, Academy of Mathematics and Systems Science, Chinese Academy of Sciences, Beijing 100190, China (lipeijun@lsec.cc.ac.cn).
§Corresponding author. State Key Laboratory of Mathematical Sciences, Academy of Mathematics and Systems Science, Chinese Academy of Sciences, Beijing 100190, China, and School of Mathematical Sciences, University of Chinese Academy of Sciences, Beijing 100049, China (wangxu@lsec.cc.ac.cn).

order TFDE is the multiterm TFDE. Multiterm TFDEs provide a versatile framework to model systems exhibiting multiple relaxation or memory time scales, which are common in various natural phenomena.

In this paper, we consider the following stochastic multiterm time-fractional diffusion-wave equation driven by a fractional Brownian motion (fBm):

$$
\begin{cases}
\displaystyle\sum_{k=1}^{n} \partial_t^{\alpha_k} u(x,t) - \partial_{xx} u(x,t) = f(t)\dot{B}^H(x), & (x,t) \in D \times \mathbb{R}_+, \\
u(x,0) = 0, & x \in \overline{D}, \\
\partial_t u(x,0) = 0, & x \in \overline{D}, \quad \text{if} \quad \alpha_n \in (1,2], \\
\partial_x u(0,t) = 0, \ u(1,t) = 0, & t \in \mathbb{R}_+,
\end{cases}
\tag{1.1}
$$

where $\partial_t^{\alpha_k}$ denotes the Caputo fractional derivative with order $\alpha_k \in (0,2]$ satisfying $\alpha_1 < \alpha_2 < \cdots < \alpha_n$ and $\alpha_1 < 2$. The domain $D := (0,1)$. The diffusion coefficient f, referred to as the source function, is a deterministic function satisfying $f(0) = 0$. Here, B^H represents the spatial fBm with a Hurst index $H \in (0,1)$, and $\dot{B}^H$ represents the formal derivative of B^H with respect to the spatial variable x.

Extensive research has been undertaken on deterministic sources for multiterm TFDEs, including both direct and inverse source problems. For instance, multivariate Mittag–Leffler functions were utilized in [7] to represent solutions of the initial boundary value problem. In [19], innovative techniques were introduced for deriving analytical solutions. The investigation of well-posedness and long-term asymptotic behavior of the initial boundary value problem was addressed in [24]. A strong maximum principle was established in [26], demonstrating uniqueness in determining the temporal component of the source term. In [23], the authors focused on the identification of time-dependent source terms using boundary data. In [20], the spatially dependent sources were successfully recovered using final data.

Due to the inherent uncertainties in practical problems, researchers have directed considerable attention to the investigation of stochastic models. In contrast to deterministic inverse problems, stochastic inverse problems are confronted with additional challenges due to the presence of randomness and uncertainty. Recently, significant progress has been made in solving inverse random source problems related to TFDEs. Research efforts have mainly focused on addressing two distinct categories of noise: time-dependent and spatial-dependent. In the case of time-dependent noise, Niu, Helin, and Zhang [30] explored scenarios involving a random source expressed as $f(x)h(t) + g(x)\dot{B}(t)$ by utilizing statistical information derived from the final data. Expanding upon this line of research, Feng, Li, and Wang [11] broadened the scope of their investigation to contain situations featuring a random source in the form of $f(x)h(t) + g(x)\dot{B}^H(t)$. Additionally, in [12, 25], the specific case involving a random source $f(x)(g_1(t)+g_2(t)\dot{B}(t))$ was examined. Lassas, Li, and Zhang [22] studied the general case characterized by a random source given by $I_t^\delta(f_1(x)g_1(t) + f_2(x)g_2(t)\dot{B}(t))$, where I_t^δ represents the Riemann–Liouville fractional integral operator. In contrast, research on spatial-dependent noise is relatively limited. An exception to this is the work of Gong et al. [16], where they conducted a detailed analysis of a TFDE with $\alpha \in (0,1)$, characterized by a random source represented as $f(t)\dot{B}(x)$.

This paper is dedicated to solving the problem (1.1) involving the multiterm TFDE with the random source $f(t)\dot{B}^H(x)$. When the Hurst parameter $H = \frac{1}{2}$, the fBm $B^H(x)$ reduces to the classical Brownian motion $B(x)$, and the random source becomes $f(t)\dot{B}(x)$. The fBm is utilized to describe complex systems with memory and long-range dependence, and it has important applications in various fields, including hydrology and geophysics [21, 27], financial mathematics [1, 13], biomedical applications [17], and material science [10, 33]. Furthermore, the multiterm TFDE considered here can also be reduced to the single-term case, i.e., the classical TFDE with the fractional derivative order $0 < \alpha < 2$, which includes subdiffusion ($0 < \alpha < 1$), superdiffusion ($1 < \alpha < 2$), and heat conduction ($\alpha = 1$). Therefore, our research can be viewed as an extension of the prior work presented in [16]. The central challenge of our study lies in dealing with the complexities introduced by fBm. To date, there is limited research on the inverse random source problem with a source driven by fBm. In [11], an inverse random source problem was examined for the TFDE with $0 < \alpha < 1$, where the random source was given as $f(x)h(t) + g(x)\dot{B}^H(t)$. To handle stochastic integration, the moving average representation of fBm was employed to convert the variance of random integrals into deterministic integrals. However, the integrals transformed using this technique were notably complex, requiring the resolution of numerous singular integrals.

In this study, we adopt the harmonizable representation, as described in [9], to address our problem. The harmonizable representation enables us to express the variance of random integrals in a more concise manner. Utilizing a crucial modified isometry formula, as presented in Lemma 3.4, we establish the well-posedness of the solution for the direct problem, which is summarized in the following theorem.

Theorem 1.1. *Assuming that $f \in \mathscr{H}^2(\mathbb{R}_+)$, the direct source problem (1.1) has a unique solution $u \in L^2(\Omega; \mathscr{H}^2(\mathbb{R}_+; L^2(D)))$, which satisfies*

$$\mathbb{E}\left[\|u\|^2_{\mathscr{H}^2(\mathbb{R}_+;L^2(D))}\right] \leqslant C\|f\|^2_{\mathscr{H}^2(\mathbb{R}_+)}, \tag{1.2}$$

where $C > 0$ is a constant depending only on H.

For the inverse problem, the uniqueness can be established for determining the phaseless Fourier modes of f:

$$|\hat{f}(\omega)| = \left(\frac{\mathbb{V}[\hat{u}(0,\omega)]}{R(\omega)}\right)^{\frac{1}{2}}, \quad \omega \in \mathbb{R},$$

where $\mathbb{V}[\cdot]$ denotes the variance of a random variable and $R(\omega)$ is defined in (4.2). However, the recovery of $|\hat{f}(\omega)|$ is unstable, as stated in the following theorem.

Theorem 1.2. *For $H \in [\frac{1}{2}, 1)$ and $|\omega| > 1$, there exists a constant $C > 0$ independent of ω and H such that*

$$R(\omega) \leqslant \frac{C}{\sin(\frac{\pi\alpha_{\max}}{2})}\left(\frac{c_H^2}{1-H} + 2\pi c_H^2\right)|\omega|^{-\alpha_{\max}},$$

where $\alpha_{\max} := \max_{i=1,\cdots,n}\{\alpha_i : \alpha_i \neq 2\}$ and $c_H := (\frac{H\Gamma(2H)\sin(H\pi)}{\pi})^{\frac{1}{2}}$. For $H \in (0, \frac{1}{2})$, assuming additionally that $\alpha_n < 2$, it holds that

$$\lim_{|\omega|\to\infty} R(\omega) = 0.$$

To validate our theoretical findings, we conduct numerical experiments for (1.1) with two time-fractional terms, addressing cases of both subdiffusion and superdiffusion simultaneously. Given that the available data is the modulus in the frequency domain and the problem is inherently ill-posed, it necessitates the resolution of a phase retrieval problem. To address this challenge, we adopt the PhaseLift algorithm, in conjunction with a spectral cut-off technique, to reconstruct the source function. Our numerical results demonstrate the effectiveness of the proposed method in handling both smooth and nonsmooth source functions.

This paper is structured as follows. Section 2 provides some necessary background information to facilitate the main results. The well-posedness of the direct problem is demonstrated in section 3. Section 4 provides a proof of uniqueness and a characterization of the ill-posed nature of the inverse problem. In section 5, we introduce the PhaseLift method for solving the inverse problem, supported by numerical examples to confirm the theoretical results. Finally, in section 6, we conclude with a summary of our study and offer suggestions for future research directions.

2. Preliminaries.

In this section, we provide a brief introduction to fBm and the Caputo fractional derivative.

2.1. Fractional Brownian motion.

A centered Gaussian process $B^H = \{B^H(x) : x \in \mathbb{R}\}$, defined on a probability space that comprises a complete triple $(\Omega, \mathcal{F}, \mathbb{P})$, is an fBm characterized by a Hurst index $H \in (0,1)$ when it exhibits the covariance function, as presented in [31] or [35]:

$$\mathcal{R}_H(x,y) := \mathbb{E}\left[B^H(x)B^H(y)\right] = \frac{1}{2}\left(|x|^{2H} + |y|^{2H} - |x-y|^{2H}\right), \quad x, y \in \mathbb{R}.$$

In order to streamline the formulation of moments for the stochastic integral, we introduce a specific integral representation of B^H in relation to a complex Gaussian measure defined over the entire real line $\mathbb{R}$.

Lemma 2.1 (cf. [35]). *The fBm B^H with $H \in (0,1)$ has the integral representation given by*

$$B^H(x) = c_H \int_{-\infty}^{\infty} \frac{e^{\mathrm{i}\lambda x} - 1}{\mathrm{i}\lambda |\lambda|^{H-\frac{1}{2}}} \mathrm{d}\widetilde{W}(\lambda), \quad x \in \mathbb{R}, \tag{2.1}$$

where the constant c_H is given in Theorem 1.2 and $\widetilde{W} = W_1 + \mathrm{i}W_2$ represents a complex Gaussian measure. Here, W_1 and W_2 are independent Gaussian measures that are independently scattered over $\mathbb{R}_+$, and they satisfy the properties $W_1(A) = W_1(-A)$ and $W_2(A) = -W_2(-A)$ for any Borel set A of finite Lebesgue measure.

The expression presented in (2.1) is commonly referred to as the harmonizable representation, also known as the spectral representation (cf. [31]).

2.2. Caputo fractional derivative.

For $\nu \in \mathbb{R}_+ \backslash \mathbb{N}$, the νth order Caputo fractional derivative of a function v is denoted as

$$\partial_t^\nu v(t) = \frac{1}{\Gamma(n-\nu)} \int_0^t (t-\xi)^{n-\nu-1} v^{(n)}(\xi) \mathrm{d}\xi,$$

where the Gamma function $\Gamma(\alpha) = \int_0^\infty e^{-s} s^\alpha \mathrm{d}s$, and $n = \lceil \nu \rceil$ with $\lceil \cdot \rceil$ denoting the smallest positive integer that is larger than or equal to ν. If $\nu \in \mathbb{N}$, $\partial_t^\nu v(t)$ denotes the classical νth order derivative, also denoted by $v^{(\nu)}(t) = \partial_t^\nu v(t)$.

Next, we examine the Fourier transform of the Caputo fractional derivative.

Lemma 2.2 (cf. [8]). *Let $\nu \in \mathbb{R}_+$, and consider a causal function $v(t)$, where $v(t) = 0$ for $t \le 0$, and $\sum_{k=0}^{n-1} |v^{(k)}(0)| = 0$ with $n = \lceil \nu \rceil$. Additionally, assume that $v^{(k)}(t)$ has compact support for all $k = 0, \dots, n$. Under these conditions, the fractional derivative $\partial_t^\nu v$ of v is well-defined in $L^2(\mathbb{R})$, and its Fourier transform satisfies*

$$\mathscr{F}[\partial_t^\nu v(\cdot)](\omega) = (\mathrm{i}\omega)^\nu \hat{v}(\omega),$$

where $\hat{v}(\omega) := \mathscr{F}[v(\cdot)](\omega)$ denotes the Fourier transform of v.

Note that the complex number $(\mathrm{i}\omega)^\nu$ may be multivalued when ν is a fractional number. Throughout, we always adopt its principal value and represent it as

$$(\mathrm{i}\omega)^\nu = |\omega|^\nu e^{\mathrm{i}\frac{\pi\nu}{2}\mathrm{sgn}(\omega)} = |\omega|^\nu \left(\cos\left(\frac{\pi\nu}{2}\right) + \mathrm{sgn}(\omega)\mathrm{i}\sin\left(\frac{\pi\nu}{2}\right)\right),$$

where $\mathrm{sgn}(\cdot)$ denotes the sign function.

3. The direct problem.

This section establishes the well-posedness of the direct source problem. First, we convert it into an equivalent problem in the frequency domain, where the existence, uniqueness, and regularity of the mild solution are investigated. We then attain the well-posedness of the time-domain problem (1.1).

3.1. The problem in the frequency domain.

For a function $v \in L^2(\mathbb{R}_+)$, we consider its zero extension outside of $\mathbb{R}_+$, still denoted by v, such that its Fourier transform $\hat{v}$ is well-defined. Taking the Fourier transform of (1.1) and applying Lemma 2.2, we obtain the following stochastic differential equation in the frequency domain, where $x \in D$ and $\omega \in \mathbb{R}$:

$$\begin{cases} \partial_{xx}\hat{u}(x,\omega) - \sum_{k=1}^{n} (\mathrm{i}\omega)^{\alpha_k} \hat{u}(x,\omega) = -\hat{f}(\omega)\dot{B}^H(x), \\ \partial_x \hat{u}(0,\omega) = 0, \quad \hat{u}(1,\omega) = 0, \end{cases} \tag{3.1}$$

where $\hat{u}$ and $\hat{f}$ are the Fourier transforms of u and f with respect to t, respectively.

For simplicity, we denote

$$s := \sum_{k=1}^{n} (\mathrm{i}\omega)^{\alpha_k} = \sum_{k=1}^{n} |\omega|^{\alpha_k} e^{\mathrm{i}\frac{\pi\alpha_k}{2}\mathrm{sgn}(\omega)} = \sum_{k=1}^{n} |\omega|^{\alpha_k} \left(\cos\left(\frac{\pi\alpha_k}{2}\right) + \mathrm{sgn}(\omega)\mathrm{i}\sin\left(\frac{\pi\alpha_k}{2}\right)\right), \tag{3.2}$$

which has the following properties.

Lemma 3.1. *For the parameter s as defined in (3.2), it holds that $s = 0$ if and only if $\omega = 0$. Furthermore,*

$$|s| \geqslant \sin\left(\frac{\pi\alpha_{\max}}{2}\right) |\omega|^{\alpha_{\max}},$$

where $\alpha_{\max}$ is defined in Theorem 1.2.

Proof. If $\omega = 0$, it is evident that $s = 0$. It is adequate to demonstrate that $\omega = 0$ when $s = 0$.

Assuming, by contradiction, that $\omega \neq 0$, it is important to note that $\frac{\pi\alpha_k}{2} \in (0, \pi]$ and, therefore, $\sin(\frac{\pi\alpha_k}{2}) \geqslant 0$ for any $\alpha_k \in (0, 2]$ and $k = 1, \ldots, n$. If

$$s = \sum_{k=1}^{n} |\omega|^{\alpha_k} \left(\cos\left(\frac{\pi\alpha_k}{2}\right) + \mathrm{sgn}(\omega)\mathrm{i}\sin\left(\frac{\pi\alpha_k}{2}\right)\right) = 0,$$

then its imaginary part $\Im[s]$ must also be zero, i.e., $\Im[s] = \mathrm{sgn}(\omega)\mathrm{i}\sum_{k=1}^{n} |\omega|^{\alpha_k} \sin(\frac{\pi\alpha_k}{2}) = 0$, which implies that $\alpha_k = 2$ for all $k = 1, \ldots, n$. Substituting $\alpha_k = 2$ into the expression for s, we obtain

$$s = \sum_{k=1}^{n} |\omega|^2 \cos(\pi) = -n\omega^2 = 0,$$

which leads to a contradiction to the assumption $\omega \neq 0$. We then establish the equivalence between $s = 0$ and $\omega = 0$.

Next, we proceed to estimate the lower bound of $|s|$. Given that $0 < \alpha_1 < \alpha_2 < \cdots < \alpha_n \leqslant 2$, we have $\sin(\frac{\pi\alpha_k}{2}) > 0, k = 1, \ldots, n-1$, and $\sin(\frac{\pi\alpha_n}{2}) \geqslant 0$. Consequently, we can deduce

$$|s| \geqslant |\Im[s]| = \sum_{k=1}^{n} |\omega|^{\alpha_k} \sin\left(\frac{\pi\alpha_k}{2}\right) \geqslant \sin\left(\frac{\pi\alpha_{\max}}{2}\right) |\omega|^{\alpha_{\max}},$$

which completes the proof. ∎

3.2. The Green function. Let $G_\omega(x, y)$ be the Green function of (3.1) for any fixed $\omega \in \mathbb{R}$. It solves the following problem (cf. [16]):

$$\begin{cases} \partial_{xx} G_\omega(x, y) - sG_\omega(x, y) = \delta(x - y), \\ \partial_x G_\omega(0, y) = 0, \quad G_\omega(1, y) = 0, \end{cases}$$

where $x, y \in D$ and the frequency s is given in (3.2). It is shown in [16] that the Green function $G_\omega(x, y)$ admits the following expression:

$$G_\omega(x, y) = \begin{cases} \max\{x, y\} - 1, & \omega = 0, \\ \dfrac{e^{\sqrt{s}(x+y)} + e^{\sqrt{s}|x-y|} - e^{\sqrt{s}(2-x-y)} - e^{\sqrt{s}(2-|x-y|)}}{2\sqrt{s}\left(1 + e^{2\sqrt{s}}\right)}, & \omega \neq 0, \end{cases} \tag{3.3}$$

where we choose the principal value for $\sqrt{s} = |s|^{\frac{1}{2}} e^{\mathrm{i}\frac{\arg(s)}{2}}$ with $\arg(\cdot)$ representing the argument with a radiant principal value in $(-\pi, \pi]$ to ensure that its real part $\Re[\sqrt{s}] > 0$ for $\omega \in \mathbb{R} \setminus \{0\}$.

Lemma 3.2. *For any $x \in \overline{D}$, the Green function G_ω provided in (3.3) satisfies*

$$\sup_{\omega\in\mathbb{R}} \|G_\omega(x, \cdot)\|_{L^2(D)} \leqslant C, \quad \sup_{\omega\in\mathbb{R}} \|G_\omega\|_{L^2(D\times D)} \leqslant C.$$

Additionally, as $|s| \to \infty$, the following inequalities hold:

$$\|G_\omega(x, \cdot)\|_{L^2(D)} \leqslant C|s|^{-\frac{1}{2}}, \quad \|G_\omega\|_{L^2(D\times D)} \leqslant C|s|^{-\frac{1}{2}},$$

where C denotes positive constants that are independent of ω and x.

Proof. It is only necessary to demonstrate that the above results apply to $\|G_\omega(x,\cdot)\|_{L^2(D)}$, as the results for $\|G_\omega\|_{L^2(D\times D)}$ follow directly.

If $\omega = 0$, it is evident that for any $x \in \overline{D}$

$$\|G_0(x,\cdot)\|^2_{L^2(D)} = \int_0^x (x-1)^2 \mathrm{d}y + \int_x^1 (y-1)^2 \mathrm{d}y = \frac{(x-1)^2(2x+1)}{3} \leqslant \frac{1}{3}.$$

If $\omega \neq 0$, using (3.3) and noting the inequality for $x, y \in (0,1)$ (cf. [16, (3.4)]),

$$|G_\omega(x,y)|^2 \leq \frac{e^{2\Re[\sqrt{s}](x+y)} + e^{2\Re[\sqrt{s}]|x-y|} + e^{2\Re[\sqrt{s}](2-x-y)} + e^{2\Re[\sqrt{s}](2-|x-y|)}}{|\sqrt{s}\left(1+e^{2\sqrt{s}}\right)|^2}, \tag{3.4}$$

where $\Re[\cdot]$ denotes the real part of a complex number, we deduce from a simple calculation that

$$\begin{aligned}
\|G_\omega(x,\cdot)\|^2_{L^2(D)} &= \int_0^1 |G_\omega(x,y)|^2 \,\mathrm{d}y \leqslant |s|^{-1} \frac{1}{|1+e^{2\sqrt{s}}|^2} \frac{e^{4\Re[\sqrt{s}]}-1}{\Re[\sqrt{s}]} \\
&= |s|^{-1} \frac{1}{1+e^{4\Re[\sqrt{s}]} + 2e^{2\Re[\sqrt{s}]} \cos\left(2\Re[\sqrt{s}] \tan\left(\frac{\arg(s)}{2}\right)\right)} \frac{e^{4\Re[\sqrt{s}]}-1}{\Re[\sqrt{s}]} \\
&=: |s|^{-1} h\left(\Re[\sqrt{s}]\right), \qquad (3.5)
\end{aligned}$$

where h is a positive function for any $\Re[\sqrt{s}] > 0$. Note that

$$\begin{aligned}
\left|h\left(\Re[\sqrt{s}]\right)\right| &= \left| \frac{1}{\Re[\sqrt{s}]} \frac{e^{4\Re[\sqrt{s}]}-1}{1+e^{4\Re[\sqrt{s}]} + 2e^{2\Re[\sqrt{s}]} \cos\left(2\Re[\sqrt{s}] \tan\left(\frac{\arg(s)}{2}\right)\right)} \right| \\
&\leqslant \left| \frac{1}{\Re[\sqrt{s}]} \frac{e^{4\Re[\sqrt{s}]}-1}{1+e^{4\Re[\sqrt{s}]} - 2e^{2\Re[\sqrt{s}]}} \right| \qquad (3.6) \\
&= \left| \frac{1}{\Re[\sqrt{s}]} \frac{e^{2\Re[\sqrt{s}]}+1}{e^{2\Re[\sqrt{s}]}-1} \right| \leqslant \frac{2}{\Re[\sqrt{s}]} \to 0, \quad \Re[\sqrt{s}] \to \infty,
\end{aligned}$$

and $\lim_{\Re[\sqrt{s}]\to 0} h\left(\Re[\sqrt{s}]\right) = 1$. Following the same procedure as in [16, Lemma 3.1], we can obtain the uniform boundedness of the function h over $[0,\infty)$. Hence,

$$\|G_\omega(x,\cdot)\|_{L^2(D)} \leqslant C|s|^{-\frac{1}{2}}, \quad \omega \in \mathbb{R}. \tag{3.7}$$

On the other hand, for any fixed $x \neq y$, when considering $G_\omega(x,y)$ as a function of s, it is analytic with respect to s and is continuous at $s = \omega = 0$, implying that

$$\lim_{\omega\to 0} G_\omega(x,y) = G_0(x,y).$$

As a consequence,

$$\|G_\omega(x,\cdot)\|_{L^2(D)} \leqslant C, \quad |s| \ll 1,$$

which, together with (3.7), finishes the proof. ∎

For the sake of convenience in notation, we introduce a function $\mathscr{T}G_\omega$ defined in $\mathbb{R}\times\mathbb{R}$ as follows:

$$\mathscr{T}G_\omega(x,y) := \begin{cases} \partial_y G_\omega(x,y), & x\in D,\ y\in[0,x)\cup(x,1], \\ 0 & \text{otherwise.} \end{cases}$$

Lemma 3.3. *The function $\mathscr{T}G_\omega \in L^2(\mathbb{R}\times\mathbb{R})$ is uniformly bounded with respect to $\omega\in\mathbb{R}$, satisfying*

$$\sup_{\omega\in\mathbb{R}} \|\mathscr{T}G_\omega\|_{L^2(\mathbb{R}\times\mathbb{R})} \leqslant C.$$

Moreover, for any fixed $x\in D$, it holds that

$$\sup_{\omega\in\mathbb{R}} \|\mathscr{T}G_\omega(x,\cdot)\|_{L^2(\mathbb{R})} \leqslant C.$$

In the above expressions, the positive constants denoted by C are independent of both ω and x.

Proof. It suffices to consider $x,y\in D$. If $\omega=0$, then

$$\mathscr{T}G_0(x,y) = \begin{cases} 0, & y\in[0,x], \\ 1, & y\in(x,1]. \end{cases}$$

A simple calculation yields

$$\|\mathscr{T}G_0(x,\cdot)\|^2_{L^2(\mathbb{R})} = \int_x^1 1\mathrm{d}y = 1-x \leqslant 1$$

and

$$\|\mathscr{T}G_0\|^2_{L^2(\mathbb{R}\times\mathbb{R})} = \|\mathscr{T}G_0\|^2_{L^2(D\times D)} = \int_0^1\int_x^1 1^2\mathrm{d}y\mathrm{d}x = \frac{1}{2}.$$

If $\omega\neq 0$, then for $x\in D,\ y\in[0,x)\cup(x,1]$, it holds that

$$\mathscr{T}G_\omega(x,y) = \frac{e^{\sqrt{s}(x+y)} - \operatorname{sgn}(x-y)e^{\sqrt{s}|x-y|} + e^{\sqrt{s}(2-x-y)} - \operatorname{sgn}(x-y)e^{\sqrt{s}(2-|x-y|)}}{2\left(1+e^{2\sqrt{s}}\right)}.$$

Similarly, we may obtain from (3.4)–(3.5) that

$$\begin{aligned} \|\mathscr{T}G_\omega(x,\cdot)\|^2_{L^2(\mathbb{R})} &\leqslant \frac{1}{\left|1+e^{2\sqrt{s}}\right|^2}\frac{e^{4\Re[\sqrt{s}]}-1}{\Re[\sqrt{s}]} \\ &= \frac{1}{1+e^{4\Re[\sqrt{s}]}+2e^{2\Re[\sqrt{s}]}\cos\left(2\Re[\sqrt{s}]\tan\left(\frac{\arg(s)}{2}\right)\right)}\frac{e^{4\Re[\sqrt{s}]}-1}{\Re[\sqrt{s}]} \\ &= h\left(\Re[\sqrt{s}]\right) \end{aligned} \tag{3.8}$$

and

$$\|\mathscr{T}G_\omega\|^2_{L^2(\mathbb{R}\times\mathbb{R})} = \int_D \|\mathscr{T}G_\omega(x,\cdot)\|^2_{L^2(\mathbb{R})}\mathrm{d}x \leqslant \int_D \frac{1}{\left|1+e^{2\sqrt{s}}\right|^2}\frac{e^{4\Re[\sqrt{s}]}-1}{\Re[\sqrt{s}]}\mathrm{d}x = h\left(\Re[\sqrt{s}]\right),$$

where h is defined in (3.5) and is uniformly bounded. Hence, there exists a constant $C>0$ independent of ω and x such that

$$\|\mathscr{T}G_\omega(x,\cdot)\|^2_{L^2(\mathbb{R})} \leqslant h(\Re[\sqrt{s}]) \leqslant C, \quad \|\mathscr{T}G_\omega\|^2_{L^2(\mathbb{R}\times\mathbb{R})} \leqslant h(\Re[\sqrt{s}]) \leqslant C,$$

which completes the proof. ∎

For any fixed $x \in D$, we denote by $\tilde{G}_\omega(x,\cdot)$ the zero extension of $G_\omega(x,\cdot)$ outside of D. Similarly, we denote $\hat{\tilde{G}}_\omega(x,\cdot)$ as the Fourier transform of $\tilde{G}_\omega(x,\cdot)$ with respect to the second variable and apply the same notation to $\widehat{\mathscr{T}G}_\omega(x,\cdot)$. Recall the definition of the fractional Sobolev space $\mathscr{H}^\gamma(\mathbb{R})$ with $\gamma\in\mathbb{R}$ (cf. [29]),

$$\mathscr{H}^\gamma(\mathbb{R}) := \left\{u\in L^2(\mathbb{R}) : \int_{\mathbb{R}} \left(1+|\zeta|^2\right)^\gamma |\hat{u}(\zeta)|^2\mathrm{d}\zeta < \infty\right\},$$

which is equipped with the norm

$$\|u\|_{\mathscr{H}^\gamma(\mathbb{R})} := \left(\int_{\mathbb{R}} \left(1+|\zeta|^2\right)^\gamma |\hat{u}(\zeta)|^2\mathrm{d}\zeta\right)^{\frac{1}{2}}.$$

Based on the above notation, we establish the following Itô isometry type equality for the stochastic integral of G_ω with respect to the fBm. This result is derived using a procedure similar to the one employed in [9, Chapter 2.2].

Lemma 3.4. *For any fixed $x\in\overline{D}$ and $H\in(0,1)$, the stochastic integral $\int_D G_\omega(x,y)\mathrm{d}B^H(y)$ is well-defined and satisfies*

$$\mathbb{E}\left[\left|\int_D G_\omega(x,y)\mathrm{d}B^H(y)\right|^2\right] = c_H^2\int_{\mathbb{R}}\frac{|\hat{\tilde{G}}_\omega(x,\zeta)|^2}{|\zeta|^{2H-1}}\mathrm{d}\zeta, \tag{3.9}$$

where c_H is defined in Lemma 2.1.

Proof. For the case where $H=\frac{1}{2}$ and $c_H^2=\frac{1}{2\pi}$, the result in (3.9) follows from the classical Itô isometry and Parseval's theorem, which states that

$$\mathbb{E}\left[\left|\int_D G_\omega(x,y)\mathrm{d}B^{\frac{1}{2}}(y)\right|^2\right] = \int_{\mathbb{R}}|\tilde{G}_\omega(x,y)|^2\mathrm{d}y = \frac{1}{2\pi}\int_{\mathbb{R}}|\hat{\tilde{G}}_\omega(x,\zeta)|^2\mathrm{d}\zeta.$$

For $H\in(\frac{1}{2},1)$, it is shown in [9, section 2.2, Case 1] that (3.9) holds if $\tilde{G}_\omega(x,\cdot)\in L^1(\mathbb{R})\cap L^2(\mathbb{R})$ for any $x\in\overline{D}$. Given that $\tilde{G}_\omega(x,\cdot)$ is supported in D and $L^2(D)\subset L^1(D)$, it is sufficient to show that $G_\omega(x,\cdot)\in L^2(D)$, which has already been demonstrated in Lemma 3.2.

For $H\in(0,\frac{1}{2})$, we cannot directly apply the conclusion from [9, section 2.2, Case 2] because $\tilde{G}_\omega(x,\cdot)\notin\mathscr{H}^1(\mathbb{R})$. In the following, we demonstrate that (3.9) still holds even under a weaker regularity condition for $\tilde{G}_\omega(x,\cdot)$.

First, we assert that $\tilde{G}_\omega(x,\cdot)\in\mathscr{H}^{\frac{1}{2}-H}(\mathbb{R})$ for any $H\in(0,\frac{1}{2})$. In fact, for any fixed $\epsilon>0$, it follows from Plancherel's theorem that

$$\begin{aligned}
&\left\|\tilde{G}_\omega(x,\cdot)\right\|^2_{\mathscr{H}^{\frac{1}{2}-H}(\mathbb{R})}\\
&=\int_{\mathbb{R}}\left(1+|\zeta|^2\right)^{\frac{1}{2}-H}|\hat{\tilde{G}}_\omega(x,\zeta)|^2\mathrm{d}\zeta\\
&=\int_{(-\epsilon,\epsilon)}\left(1+|\zeta|^2\right)^{\frac{1}{2}-H}|\hat{\tilde{G}}_\omega(x,\zeta)|^2\mathrm{d}\zeta+\int_{\mathbb{R}\setminus(-\epsilon,\epsilon)}\left(1+|\zeta|^2\right)^{\frac{1}{2}-H}|\hat{\tilde{G}}_\omega(x,\zeta)|^2\mathrm{d}\zeta\\
&\leqslant\left(1+\epsilon^2\right)^{\frac{1}{2}-H}\|\hat{\tilde{G}}_\omega(x,\cdot)\|^2_{L^2(\mathbb{R})}+\int_{\mathbb{R}\setminus(-\epsilon,\epsilon)}\left(\frac{1}{|\zeta|^2}+1\right)^{\frac{1}{2}-H}|\zeta|^{1-2H}|\hat{\tilde{G}}_\omega(x,\zeta)|^2\mathrm{d}\zeta\\
&\leqslant 2\pi\left(1+\epsilon^2\right)^{\frac{1}{2}-H}\|G_\omega(x,\cdot)\|^2_{L^2(D)}+\left(\frac{1}{\epsilon^2}+1\right)^{\frac{1}{2}-H}\int_{\mathbb{R}\setminus(-\epsilon,\epsilon)}|\zeta|^{-2H-1}|\zeta\hat{\tilde{G}}_\omega(x,\zeta)|^2\mathrm{d}\zeta,
\end{aligned}$$

where $\|G_\omega(x,\cdot)\|_{L^2(D)}<\infty$, as shown in Lemma 3.2, and

$$\begin{aligned}
&\int_{\mathbb{R}\setminus(-\epsilon,\epsilon)}|\zeta|^{-2H-1}|\zeta\hat{\tilde{G}}_\omega(x,\zeta)|^2\mathrm{d}\zeta\\
&=\int_{\mathbb{R}\setminus(-\epsilon,\epsilon)}|\zeta|^{-2H-1}\left|\zeta\int_0^x G_\omega(x,y)e^{-\mathrm{i}\zeta y}\mathrm{d}y+\zeta\int_x^1 G_\omega(x,y)e^{-\mathrm{i}\zeta y}\mathrm{d}y\right|^2\mathrm{d}\zeta\\
&=\int_{\mathbb{R}\setminus(-\epsilon,\epsilon)}|\zeta|^{-2H-1}\left|\left(G_\omega(x,y)e^{-\mathrm{i}\zeta y}\right)\Big|_{y=0}^{x}-\int_0^x\partial_y G_\omega(x,y)e^{-\mathrm{i}\zeta y}\mathrm{d}y\right.\\
&\quad\left.+\left(G_\omega(x,y)e^{-\mathrm{i}\zeta y}\right)\Big|_{y=x}^{1}-\int_x^1\partial_y G_\omega(x,y)e^{-\mathrm{i}\zeta y}\mathrm{d}y\right|^2\mathrm{d}\zeta\\
&=\int_{\mathbb{R}\setminus(-\epsilon,\epsilon)}|\zeta|^{-2H-1}\left|G_\omega(x,0)+\int_0^x e^{-\mathrm{i}\zeta y}\partial_y G_\omega(x,y)\mathrm{d}y+\int_x^1 e^{-\mathrm{i}\zeta y}\partial_y G_\omega(x,y)\mathrm{d}y\right|^2\mathrm{d}\zeta\\
&=\int_{\mathbb{R}\setminus(-\epsilon,\epsilon)}|\zeta|^{-2H-1}\left|G_\omega(x,0)+\widehat{\mathscr{T}G}_\omega(x,\zeta)\right|^2\mathrm{d}\zeta\\
&\leqslant\frac{2}{H}\epsilon^{-2H}|G_\omega(x,0)|^2+2\epsilon^{-2H-1}\|\mathscr{T}G_\omega(x,\cdot)\|^2_{L^2(\mathbb{R})}<\infty
\end{aligned}\tag{3.10}$$

based on Lemma 3.3.

Note that $C_0^\infty(\mathbb{R})$ is dense in $\mathscr{H}^{\frac{1}{2}-H}(\mathbb{R})$ (cf. [2, Theorem 7.38]). Therefore, for the previously claimed $\tilde{G}_\omega(x,\cdot)\in\mathscr{H}^{\frac{1}{2}-H}(\mathbb{R})$, there exists a sequence $\{\phi_n:=\phi_n^{x,\omega}\}_{n\in\mathbb{N}}\subset C_0^\infty(\mathbb{R})$ converging to $\tilde{G}_\omega(x,\cdot)$ in the norm $\|\cdot\|_{\mathscr{H}^{\frac{1}{2}-H}(\mathbb{R})}$. Moreover, according to [9, (2.8)], (3.9) holds for the sequence $\{\int_{\mathbb{R}}\phi_n(y)\mathrm{d}B^H(y)\}_{n\in\mathbb{N}}$. Hence, we obtain

$$\begin{aligned}
\mathbb{E}\left[\left|\int_{\mathbb{R}}\phi_n(y)\mathrm{d}B^H(y)-\int_{\mathbb{R}}\phi_m(y)\mathrm{d}B^H(y)\right|^2\right]&=c_H^2\int_{\mathbb{R}}\frac{\left|\hat{\phi}_n(\zeta)-\hat{\phi}_m(\zeta)\right|^2}{|\zeta|^{2H-1}}\mathrm{d}\zeta\\
&\leqslant c_H^2\int_{\mathbb{R}}\left|\hat{\phi}_n(\zeta)-\hat{\phi}_m(\zeta)\right|^2(1+|\zeta|^{1-2H})\mathrm{d}\zeta\\
&=c_H^2\|\phi_n-\phi_m\|^2_{\mathscr{H}^{\frac{1}{2}-H}(\mathbb{R})}.
\end{aligned}$$

As a result, the sequence $\{\int_{\mathbb{R}} \phi_n(y)\mathrm{d}B^H(y)\}_{n\in\mathbb{N}}$ converges in the mean square sense, and we define the stochastic integral $\int_{\mathbb{R}} \tilde{G}_\omega(x,y)\mathrm{d}B^H(y)$ as the mean square limit of $\int_{\mathbb{R}} \phi_n(y)\mathrm{d}B^H(y)$. Finally, we obtain

$$\begin{aligned}\mathbb{E}\left[\left|\int_D G_\omega(x,y)\mathrm{d}B^H(y)\right|^2\right] &= \mathbb{E}\left[\left|\int_{\mathbb{R}} \tilde{G}_\omega(x,y)\mathrm{d}B^H(y)\right|^2\right] = \lim_{n\to\infty}\mathbb{E}\left[\left|\int_{\mathbb{R}} \phi_n(y)\mathrm{d}B^H(y)\right|^2\right] \\ &= \lim_{n\to\infty} c_H^2 \int_{\mathbb{R}} \frac{|\hat{\phi}_n(\zeta)|^2}{|\zeta|^{2H-1}}\mathrm{d}\zeta = c_H^2 \int_{\mathbb{R}} \frac{|\hat{\tilde{G}}_\omega(x,\zeta)|^2}{|\zeta|^{2H-1}}\mathrm{d}\zeta,\end{aligned}$$

where the last equality follows from

$$\begin{aligned}&\left|\int_{\mathbb{R}} \frac{|\hat{\phi}_n(\zeta)|^2}{|\zeta|^{2H-1}}\mathrm{d}\zeta - \int_{\mathbb{R}} \frac{|\hat{\tilde{G}}_\omega(x,\zeta)|^2}{|\zeta|^{2H-1}}\mathrm{d}\zeta\right| \\ &\quad\leqslant \int_{\mathbb{R}} |\hat{\phi}_n(\zeta) - \hat{\tilde{G}}_\omega(x,\zeta)|\left(|\hat{\phi}_n(\zeta)| + |\hat{\tilde{G}}_\omega(x,\zeta)|\right)|\zeta|^{1-2H}\mathrm{d}\zeta \\ &\quad\leqslant \|\phi_n - \tilde{G}_\omega(x,\cdot)\|_{\mathscr{H}^{\frac{1}{2}-H}(\mathbb{R})}\left(\|\phi_n\|_{\mathscr{H}^{\frac{1}{2}-H}(\mathbb{R})} + \|\tilde{G}_\omega(x,\cdot)\|_{\mathscr{H}^{\frac{1}{2}-H}(\mathbb{R})}\right) \to 0\end{aligned}$$

as $n\to\infty$ due to the convergence of $\{\phi_n\}_{n\in\mathbb{N}}$ to $\tilde{G}_\omega(x,\cdot)$ in $\mathscr{H}^{\frac{1}{2}-H}(\mathbb{R})$. ∎

Corollary 3.5. *For a given $H\in(0,1)$, the following inequality holds:*

$$\sup_{\omega\in\mathbb{R}}\int_D \mathbb{E}\left[\left|\int_D G_\omega(x,y)\mathrm{d}B^H(y)\right|^2\right]\mathrm{d}x \leqslant C,$$

where C is a positive constant depending only on H.

Proof. The result for $H=\frac{1}{2}$ follows from Lemmas 3.2 and 3.4.

For $H\in(\frac{1}{2},1)$, utilizing Lemma 3.4, Plancherel's theorem, and the observation

$$|\hat{\tilde{G}}_\omega(x,\zeta)| = \left|\int_{\mathbb{R}} \tilde{G}_\omega(x,y)e^{-\mathrm{i}y\zeta}\,\mathrm{d}y\right| \leqslant \int_D |G_\omega(x,y)|\,\mathrm{d}y \leqslant \|G_\omega(x,\cdot)\|_{L^2(D)} \quad \forall\,\zeta\in\mathbb{R},$$

we have

$$\begin{aligned}\mathbb{E}\left[\left|\int_D G_\omega(x,y)\mathrm{d}B^H(y)\right|^2\right] &= c_H^2\int_{(-1,1)} \frac{|\hat{\tilde{G}}_\omega(x,\zeta)|^2}{|\zeta|^{2H-1}}\mathrm{d}\zeta + c_H^2\int_{\mathbb{R}\setminus(-1,1)} \frac{|\hat{\tilde{G}}_\omega(x,\zeta)|^2}{|\zeta|^{2H-1}}\mathrm{d}\zeta \\ &\leqslant c_H^2\|G_\omega(x,\cdot)\|_{L^2(D)}^2\int_{(-1,1)}\frac{1}{|\zeta|^{2H-1}}\,\mathrm{d}\zeta + c_H^2\|\hat{\tilde{G}}_\omega(x,\cdot)\|_{L^2(\mathbb{R})}^2 \\ &= \left(\frac{c_H^2}{1-H} + 2\pi c_H^2\right)\|G_\omega(x,\cdot)\|_{L^2(D)}^2, \qquad (3.11)\end{aligned}$$

which, together with Lemma 3.2, implies that

$$\sup_{\omega\in\mathbb{R}}\int_D \mathbb{E}\left[\left|\int_D G_\omega(x,y)\mathrm{d}B^H(y)\right|^2\right]\mathrm{d}x \leqslant C\sup_{\omega\in\mathbb{R}}\|G_\omega\|_{L^2(D\times D)}^2 \leqslant C.$$

For $H \in (0, \frac{1}{2})$, it follows from Lemma 3.4 and (3.10) that

$$\begin{aligned}\mathbb{E}\left[\left|\int_D G_\omega(x,y)\mathrm{d}B^H(y)\right|^2\right] &= c_H^2 \int_{(-1,1)} |\zeta|^{1-2H} |\hat{\tilde{G}}_\omega(x,\zeta)|^2 \mathrm{d}\zeta \\ &\quad + c_H^2 \int_{\mathbb{R}\setminus(-1,1)} |\zeta|^{-2H-1} |\zeta \hat{\tilde{G}}_\omega(x,\zeta)|^2 \mathrm{d}\zeta \\ &\leqslant c_H^2 \left(\|G_\omega(x,\cdot)\|_{L^2(D)}^2 + \frac{2}{H}|G_\omega(x,0)|^2 + 2\|\mathscr{T} G_\omega(x,\cdot)\|_{L^2(\mathbb{R})}^2 \right). \end{aligned} \tag{3.12}$$

Hence, Lemmas 3.2 and 3.3, in conjunction with the definition of $G_\omega(\cdot,0)$, lead to

$$\begin{aligned}&\sup_{\omega\in\mathbb{R}} \int_D \mathbb{E}\left[\left|\int_D G_\omega(x,y)\mathrm{d}B^H(y)\right|^2\right] \mathrm{d}x \\ &\quad \leqslant C \sup_{\omega\in\mathbb{R}} \left(\|G_\omega\|_{L^2(D\times D)}^2 + \|G_\omega(\cdot,0)\|_{L^2(D)}^2 + \|\mathscr{T} G_\omega\|_{L^2(D\times D)}^2 \right) \leqslant C,\end{aligned}$$

which concludes the proof. ∎

3.3. The well-posedness. Utilizing the Green function $G_\omega(x,y)$, the boundary value problem (3.1) has a unique mild solution in the form

$$\hat{u}(x,\omega) = -\hat{f}(\omega) \int_D G_\omega(x,y)\mathrm{d}B^H(y), \quad \omega \in \mathbb{R}, \tag{3.13}$$

which satisfies the following regularity estimate.

Lemma 3.6. *Let $p \geqslant 0$ and $f \in \mathscr{H}^p(\mathbb{R}_+)$. The solution (3.13) of the stochastic differential equation (3.1) satisfies*

$$\mathbb{E}\left[\int_{\mathbb{R}} \|(\mathrm{i}\omega)^p \hat{u}(\cdot,\omega)\|_{L^2(D)}^2 \mathrm{d}\omega\right] \leqslant C\|f\|_{\mathscr{H}^p(\mathbb{R}_+)}^2,$$

where $C > 0$ is a constant depending only on H.

Proof. By Corollary 3.5, we have

$$\begin{aligned}\mathbb{E}\left[\int_{\mathbb{R}} \|(\mathrm{i}\omega)^p \hat{u}(\cdot,\omega)\|_{L^2(D)}^2 \mathrm{d}\omega\right] &= \int_{\mathbb{R}} |(\mathrm{i}\omega)^p \hat{f}(\omega)|^2 \int_D \mathbb{E}\left[\left|\int_D G_\omega(x,y)\mathrm{d}B^H(y)\right|^2\right] \mathrm{d}x\mathrm{d}\omega \\ &\leqslant C \int_{\mathbb{R}} |(\mathrm{i}\omega)^p \hat{f}(\omega)|^2 \mathrm{d}\omega \leqslant C \int_{\mathbb{R}} (1+|\omega|^2)^p |\hat{f}(\omega)|^2 \mathrm{d}\omega = C\|f\|_{\mathscr{H}^p(\mathbb{R}_+)}^2,\end{aligned}$$

which completes the proof. ∎

Now, we are in a position to obtain the well-posedness of the original problem (1.1) based on the equivalent problem (3.1) obtained through the Fourier transform.

Proof of Theorem 1.1. The proof draws inspiration from [16]. Let $\{f(t)\}_{t\in\mathbb{R}}$ be the zero extension of $\{f(t)\}_{t\in\mathbb{R}_+}$, as initially explained in section 3.1. For any $x\in D$ and $t\in\mathbb{R}$, with $\hat{u}(x,\omega)$ considered as the mild solution of (3.1), we define the inverse Fourier transform of $\hat{u}(x,\omega)$ as follows:

$$\breve{u}(x,t) := -\int_{-\infty}^{t} f(\tau)\mathscr{F}^{-1}\left[\int_D G_\omega(x,y)\mathrm{d}B^H(y)\right](t-\tau)\mathrm{d}\tau.$$

By Plancherel's theorem and Lemma 3.6, we obtain $\partial_t\breve{u}, \partial_t^2\breve{u}\in L^2(\Omega; L^2(D\times\mathbb{R}))$ and

$$\begin{aligned}\mathbb{E}\left[\|\breve{u}\|^2_{\mathscr{H}^2(\mathbb{R};L^2(D))}\right] &= \mathbb{E}\left[\int_{\mathbb{R}}(1+|\omega|^2)^2\|\hat{u}(\cdot,\omega)\|^2_{L^2(D)}\mathrm{d}\omega\right]\\ &\leqslant \mathbb{E}\left[\int_{\mathbb{R}}\|\hat{u}(\cdot,\omega)\|^2_{L^2(D)}\mathrm{d}\omega\right] + 2\mathbb{E}\left[\int_{\mathbb{R}}\|(\mathrm{i}\omega)\hat{u}(\cdot,\omega)\|^2_{L^2(D)}\mathrm{d}\omega\right]\\ &\quad + \mathbb{E}\left[\int_{\mathbb{R}}\|(\mathrm{i}\omega)^2\hat{u}(\cdot,\omega)\|^2_{L^2(D)}\mathrm{d}\omega\right] \leqslant C\|f\|^2_{\mathscr{H}^2(\mathbb{R}_+)},\end{aligned}$$

which also implies that the Caputo fractional derivative of $\breve{u}$ with respect to the time t is properly defined.

Let $u(x,t)$ be the restriction of $\breve{u}(x,t)$ to t belonging to the set of nonnegative real numbers, i.e.,

$$u(x,t) := \breve{u}(x,t)|_{t\in\mathbb{R}_+}.$$

It can be readily verified that, in a mean square sense, the function u defined as described above is the unique mild solution of (1.1). It is clear to note that

$$u(x,0) = \breve{u}(x,0) = 0, \quad \partial_t u(x,0) = \partial_t\breve{u}(x,0) = 0.$$

In addition, it also satisfies (1.2). ∎

4. The inverse problem.

In this section, our primary focus is on addressing the uniqueness and instability in the reconstruction of the phaseless Fourier mode $|\hat{f}(\omega)|$ of the source function f from the measured data $\{u(0,t)\}_{t\geq 0}$ at the observation point $x=0$. To subsequently recover $|f(t)|$ from $|\hat{f}(\omega)|$, commonly referred to as the phase retrieval problem, we introduce and employ the PhaseLift technique.

Evaluating (3.13) at $x=0$ and then taking the expected value and variance on both sides, we deduce

$$\mathbb{E}[\hat{u}(0,\omega)] = 0, \quad \mathbb{V}[\hat{u}(0,\omega)] = R(\omega)|\hat{f}(\omega)|^2, \tag{4.1}$$

where $R(\omega)$ is a critical constant depending on ω and is given by

$$R(\omega) := \mathbb{E}\left[\left|\int_D G_\omega(0,y)\mathrm{d}B^H(y)\right|^2\right]. \tag{4.2}$$

Here, for any $y\in D$, we have

$$G_\omega(0,y) = \begin{cases} y-1, & \omega = 0,\\ \dfrac{e^{\sqrt{s}y} - e^{\sqrt{s}(2-y)}}{\sqrt{s}\left(1+e^{2\sqrt{s}}\right)}, & \omega\neq 0.\end{cases}$$

4.1. Uniqueness. It is clear to note from (4.1) that $|\hat{f}(\omega)|$ can be uniquely determined by

$$|\hat{f}(\omega)| = \left(\frac{\mathbb{V}[\hat{u}(0,\omega)]}{R(\omega)}\right)^{\frac{1}{2}}, \quad \omega \in \mathbb{R}, \tag{4.3}$$

if $R(\omega) > 0$. In fact, as stated in the following lemma, the uniqueness mentioned here is established.

Lemma 4.1. *For $H \in (0,1)$, it holds for any $\omega \in \mathbb{R}$ that $R(\omega) > 0$.*

Proof. We have from Lemma 3.4 that

$$R(\omega) = c_H^2 \int_{\mathbb{R}} \frac{|\hat{\tilde{G}}_\omega(0,\zeta)|^2}{|\zeta|^{2H-1}} \mathrm{d}\zeta \geqslant c_H^2 \int_0^1 \frac{|\hat{\tilde{G}}_\omega(0,\zeta)|^2}{\zeta^{2H-1}} \mathrm{d}\zeta,$$

where $\hat{\tilde{G}}_\omega(0,\zeta)$ with $\zeta \in (0,1)$ can be calculated as follows.

If $\omega = 0$, it holds that

$$\begin{aligned} \left|\hat{\tilde{G}}_0(0,\zeta)\right|^2 &= \left|\int_D G_0(0,y) e^{-\mathrm{i}\zeta y} \mathrm{d}y\right|^2 = \left|\int_0^1 (y-1) e^{-\mathrm{i}\zeta y} \mathrm{d}y\right|^2 \\ &= \left|\frac{e^{-\mathrm{i}\zeta} - 1 + \mathrm{i}\zeta}{\zeta^2}\right|^2 = \frac{(\cos(\zeta)-1)^2 + (\sin(\zeta)-\zeta)^2}{\zeta^4}, \end{aligned}$$

which, together with $\frac{(\cos(\zeta)-1)^2+(\sin(\zeta)-\zeta)^2}{\zeta^{2H+3}} > 0$ for any $\zeta \in (0,1)$, implies that

$$R(0) \geqslant c_H^2 \int_0^1 \frac{(\cos(\zeta)-1)^2 + (\sin(\zeta)-\zeta)^2}{\zeta^{2H+3}} \mathrm{d}\zeta > 0.$$

If $\omega \neq 0$, it follows from a straightforward calculation that

$$\begin{aligned} \hat{\tilde{G}}_\omega(0,\zeta) &= \int_D G_\omega(0,y) e^{-\mathrm{i}\zeta y} \mathrm{d}y \\ &= \frac{1}{\sqrt{s}\left(1+e^{2\sqrt{s}}\right)} \left(\frac{e^{\sqrt{s}-\mathrm{i}\zeta} - 1}{\sqrt{s} - \mathrm{i}\zeta} + \frac{e^{\sqrt{s}-\mathrm{i}\zeta} - e^{2\sqrt{s}}}{\sqrt{s} + \mathrm{i}\zeta}\right) \\ &= \frac{2\sqrt{s} e^{\sqrt{s}-\mathrm{i}\zeta} - \sqrt{s}(e^{2\sqrt{s}}+1) + \mathrm{i}\zeta(e^{2\sqrt{s}}-1)}{\sqrt{s}(1+e^{2\sqrt{s}})(s+\zeta^2)}. \end{aligned}$$

For $\omega \neq 0$, i.e., $s \neq 0$, we assert that $|\hat{\tilde{G}}_\omega(0,\zeta)| \not\equiv 0$ for $\zeta \in [0,1]$. In fact, if $\sqrt{s} \neq 2n\pi\mathrm{i}$ with $n \in \mathbb{Z} \setminus \{0\}$, then

$$|\hat{\tilde{G}}_\omega(0,0)| = \left|\frac{2e^{\sqrt{s}} - e^{2\sqrt{s}} - 1}{s\left(1+e^{2\sqrt{s}}\right)}\right| = \left|\frac{(e^{\sqrt{s}}-1)^2}{s\left(1+e^{2\sqrt{s}}\right)}\right| > 0.$$

If $\sqrt{s} = 2n\pi\mathrm{i}$ with $n \in \mathbb{Z} \setminus \{0\}$, then $e^{\sqrt{s}} = 1$ and $|\hat{\tilde{G}}_\omega(0,1)| = |\frac{e^{-\mathrm{i}}-1}{1-4n^2\pi^2}| > 0$, which finishes the assertion. As a result,

$$R(\omega) \geqslant c_H^2 \int_0^1 \frac{|\hat{\tilde{G}}_\omega(0,\zeta)|^2}{\zeta^{2H-1}} \mathrm{d}\zeta > 0$$

due to the continuity of $\hat{\tilde{G}}_\omega(0,\cdot)$ in $[0,1]$ for $\omega \neq 0$. ∎

4.2. Instability. While the uniqueness of the reconstruction for $|\hat{f}(\omega)|$ is confirmed by (4.3) and Lemma 4.1, the recovery process is unstable, as demonstrated in Theorem 1.2. In this subsection, we always assume that $|\omega| > 1$.

Proof of Theorem 1.2. The proof is split into three cases: $H = \frac{1}{2}$, $H \in (\frac{1}{2}, 1)$, and $H \in (0, \frac{1}{2})$, separately.

For $H = \frac{1}{2}$, it holds that $R(\omega) = \|G_\omega(0,\cdot)\|^2_{L^2(D)} \leqslant C|s|^{-1}$ from Lemma 3.2.

For $H \in (\frac{1}{2}, 1)$, by utilizing (3.11) and Lemma 3.2, we obtain

$$R(\omega) \leqslant \left(\frac{c_H^2}{1-H} + 2\pi c_H^2\right) \|G_\omega(0,\cdot)\|^2_{L^2(D)} \leqslant C\left(\frac{c_H^2}{1-H} + 2\pi c_H^2\right)|s|^{-1}. \tag{4.4}$$

Then, the result for the case $H \in [\frac{1}{2}, 1)$ follows directly from the fact $|s| \geqslant \sin(\frac{\pi\alpha_{\max}}{2})|\omega|^{\alpha_{\max}}$ as given in Lemma 3.1.

For $H \in (0, \frac{1}{2})$, the estimate (3.12) gives

$$R(\omega) \leqslant c_H^2 \left(\|G_\omega(0,\cdot)\|^2_{L^2(D)} + \frac{2}{H}|G_\omega(0,0)|^2 + 2\|\mathscr{T}G_\omega(0,\cdot)\|^2_{L^2(\mathbb{R})}\right),$$

where $\|G_\omega(0,\cdot)\|^2_{L^2(D)} \leqslant C|s|^{-1}$, $|G_\omega(0,0)|^2 = |\frac{1-e^{2\sqrt{s}}}{\sqrt{s}(1+e^{2\sqrt{s}})}|^2 \leqslant |s|^{-1}$, and

$$\|\mathscr{T}G_\omega(0,\cdot)\|^2_{L^2(\mathbb{R})} \leqslant h\left(\Re[\sqrt{s}]\right) \leqslant 2\left|\Re[\sqrt{s}]\right|^{-1}, \quad \Re[\sqrt{s}] \to \infty,$$

according to (3.6) and (3.8). It then suffices to estimate $|\Re[\sqrt{s}]|^{-1}$. Note that

$$\left|\Re[\sqrt{s}]\right|^{-1} = |s|^{-\frac{1}{2}}\left|\cos\left(\frac{\arg(s)}{2}\right)\right|^{-1}, \quad \left|\cos\left(\frac{\arg(s)}{2}\right)\right| = \sqrt{\frac{\cos(\arg(s))+1}{2}},$$

where

$$\cos(\arg(s)) = \frac{\Re[s]}{|s|} = \frac{\sum_{k=1}^{n}|\omega|^{\alpha_k}\cos\left(\frac{\pi\alpha_k}{2}\right)}{\sqrt{\sum_{k=1}^{n}|\omega|^{2\alpha_k} + 2\sum_{1\leqslant i<j\leqslant n}|\omega|^{\alpha_i+\alpha_j}\cos\left(\frac{\pi\alpha_i-\pi\alpha_j}{2}\right)}} \to \cos\frac{\pi\alpha_n}{2}$$

as $|\omega| \to \infty$. We then get

$$R(\omega) \leqslant c_H^2\left(C\left(1+\frac{1}{H}\right)|s|^{-1} + C|s|^{-\frac{1}{2}}\left(\frac{\cos(\arg(s))+1}{2}\right)^{-\frac{1}{2}}\right) \to 0, \quad |\omega| \to \infty, \tag{4.5}$$

which completes the proof. ∎

Theorem 1.2 implies that the reconstruction for $|\hat{f}(\omega)|$ using (4.3) is unstable. More precisely, any small perturbation in the data $\mathbb{V}[\hat{u}(0,\omega)]$ will be significantly amplified in the reconstruction when $|\omega|$ is sufficiently large. The degree of ill-posedness follows a polynomial form of $|\omega|^{-\gamma}$, where

$$\gamma = \begin{cases} \alpha_{\max}, & H \in \left[\frac{1}{2}, 1\right), \\ \frac{\alpha_{\max}}{2}, & H \in \left(0, \frac{1}{2}\right). \end{cases}$$

Based on the dependence of the estimates (4.4)–(4.5) on H, it indicates that, for both $H \in (0, \frac{1}{2})$ and $H \in [\frac{1}{2}, 1)$, the problem becomes increasingly unstable as H decreases. Furthermore, for $H \in (0, \frac{1}{2})$, if $\alpha_n = 2$, which is not covered by Theorem 1.2, the limit behavior of $R(\omega)$ remains uncertain due to the fact that $\lim_{|\omega|\to\infty} \cos(\arg(s)) = -1$ and thus

$$\lim_{|\omega|\to\infty} \cos\left(\frac{\arg(s)}{2}\right) = 0,$$

which makes the limit behavior of $|\Re[\sqrt{s}]|^{-1} = |s|^{-\frac{1}{2}}|\cos(\frac{\arg(s)}{2})|^{-1}$ unclear as $|\omega| \to \infty$.

The following remarks provide some straightforward extensions of the present results.

Remark 4.2.

(i) It is notable that the recovery formula (4.3) remains independent of the observation point. Specifically, the measured data $\{u(x_0, t)\}_{t\geq 0}$ can be selected at any observation point $x_0 \in [0, 1)$, leading to

$$|\hat{f}(\omega)| = \left(\frac{\mathbb{V}[\hat{u}(x_0, \omega)]}{R(x_0, \omega)}\right)^{\frac{1}{2}},$$

where $R(x_0, \omega) := \mathbb{E}[|\int_D G_\omega(x_0, y)\mathrm{d}B^H(y)|^2]$. The instability estimate provided in Theorem 1.2 remains valid for $R(x_0, \omega)$ under the same reasoning.

(ii) The framework can be extended to problems involving Robin or other boundary conditions. In such cases, establishing estimates for the corresponding Green function and adjusting the measured data accordingly are necessary.

5. Numerical experiments. As a representative example, we consider the two-term time-fractional stochastic diffusion-wave equation

$$\begin{cases} \partial_t^{\alpha_1} u(x,t) + \partial_t^{\alpha_2} u(x,t) - \partial_{xx} u(x,t) = f(t)\dot{B}^H(x), & (x,t) \in D \times (0,T], \\ u(x,0) = 0, & x \in D, \\ \partial_t u(x,0) = 0, & x \in D, \quad \text{if} \quad \alpha_2 \in (1,2), \\ \partial_x u(0,t) = 0, \ u(1,t) = 0, & t \in [0,T], \end{cases} \tag{5.1}$$

where $D = (0, 1)$, $T > 0$, and $\alpha_i \in (0, 2)$ for $i = 1, 2$ with $\alpha_1 < \alpha_2$. To simplify notation, we use the vector $\boldsymbol{\alpha} := [\alpha_1, \alpha_2]$.

To generate synthetic data, we employ the finite difference method presented in [37] to discretize (5.1). The numerical solution, denoted as u_0^n, serves as an approximation of the exact solution $u(0, t_n)$. Recognizing that observed data in practical scenarios are often subject to contamination from various sources, we introduce the following noisy data model:

$$u_0^{n,\epsilon} = u_0^n (1 + \epsilon\eta_n), \quad n = 0, \ldots, N, \tag{5.2}$$

where $\epsilon > 0$ represents the noise level, and $\{\eta_n\}_{n=0,\ldots,N}$ is a sequence of independent random variables uniformly distributed in $[-1, 1]$. The required data, denoted as $\hat{u}_0^{n_\omega,\epsilon}, n_\omega = 1, \ldots, N_\omega$, is generated by performing a discrete Fourier transform on the noisy data $\{u_0^{n,\epsilon}\}_{n=0,\ldots,N}$ at specific discrete frequencies $\{\omega_{n_\omega}\}_{n_\omega=1}^{N_\omega}$. The details of the frequency selection process will be presented in the numerical examples.

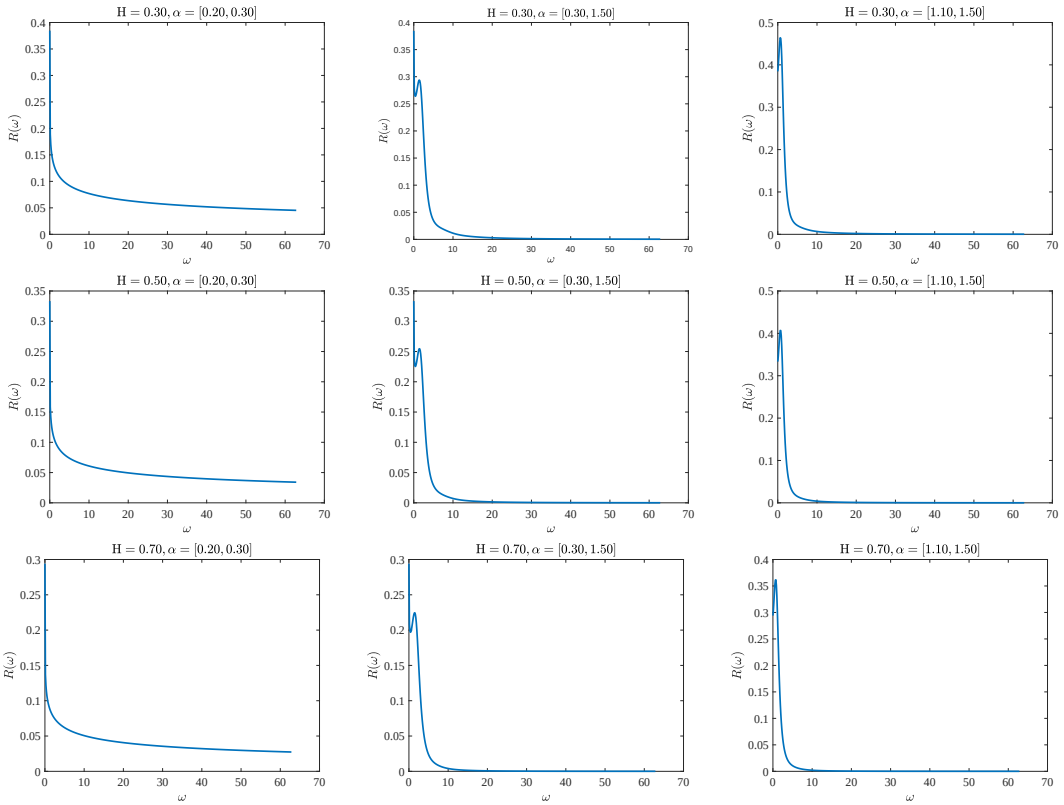

Figure 1. *The values of $R(\omega)$ for (top) $H = 0.3$, (middle) $H = 0.5$, and (bottom) $H = 0.7$ with different $\boldsymbol{\alpha}$.*

We propose a two-step method. First, the phaseless Fourier modes $\{|\hat{f}^{\epsilon}(\omega_{n_\omega})|\}_{n_\omega=1}^{N_\omega}$ are obtained from the noisy data $\{\hat{u}_0^{n_\omega,\epsilon}\}_{n_\omega=1}^{N_\omega}$ using (4.3), combined with a regularization technique. Second, the numerical approximation of $|f(t_n)|_{n=0}^{N}$ is reconstructed from $\{|\hat{f}^{\epsilon}(\omega_{n_\omega})|\}_{n_\omega=1}^{N_\omega}$ using the PhaseLift algorithm.

5.1. Spectral cut-off regularization. It is shown in section 4.1 that $|\hat{f}(\omega)|$ can be uniquely determined through (4.3). Nevertheless, the reconstruction is characterized as unstable, as elaborated in section 4.2. Consequently, a spectral cut-off regularization is employed when computing $\{|\hat{f}^{\epsilon}(\omega_{n_\omega})|\}_{n_\omega=1}^{N_\omega}$ from the noisy data $\{\hat{u}_0^{n_\omega,\epsilon}\}_{n_\omega=1}^{N_\omega}$ using the formula

$$|\hat{f}^{\epsilon}(\omega_{n_\omega})| = \left(\frac{\mathbb{V}[\hat{u}_0^{n_\omega,\epsilon}]}{R(\omega_{n_\omega})}\right)^{\frac{1}{2}}, \quad n_\omega = 1, \ldots, N_\omega. \tag{5.3}$$

To address this ill-posed problem more effectively, we define $\omega_{n_\omega} = \text{linspace}(0, W, n_\omega)$, where W serves as a regularization parameter. This choice removes high-frequency modes with $\omega > W$ from the noisy data.

Note that the second moment of the stochastic integral $R(\omega)$ involved in (4.3) is independent of the data and can be computed in advance. Figure 1 presents its values concerning ω for different values of $H = 0.3, 0.5, 0.7$. The graph illustrates that for a fixed H (resp., $\boldsymbol{\alpha}$), the value of $R(\omega)$ decreases more rapidly when α_i (resp., H) is larger. It is evident that the

choice of the regularization parameter W plays an essential role in the reconstruction, and its selection will be detailed in the subsequent numerical examples.

5.2. PhaseLift algorithm. Based on the phaseless Fourier modes $\{|\hat{f}^\epsilon(\omega_{n_\omega})|\}_{n_\omega=1}^{N_\omega}$ obtained earlier, our next objective is to obtain the approximation $\{|f^\epsilon(t_n)|\}_{n=0}^{N}$ of $\{|f(t_n)|\}_{n=0}^{N}$ from $\{|\hat{f}^\epsilon(\omega_{n_\omega})|\}_{n_\omega=1}^{N_\omega}$. This problem, which involves reconstructing the signal at discrete points from the magnitude of its discrete Fourier transform, is known as the discrete phase retrieval problem [18, 32].

The phase retrieval problem is evidently ill-posed and notoriously challenging to solve. In recent years, many researchers have demonstrated that it can be reformulated as an optimization problem. Consequently, several algorithms have been proposed to address this problem, including PhaseLift [3], PhaseCut [38], and PhaseMax [15].

The PhaseLift algorithm is employed to address our discrete phase retrieval problem, which comprises two primary components: multiple structured illumination and lifting. Multiple structured illumination is designed to obtain additional measurements by utilizing masks, optical gratings, or oblique illuminations artificially. Lifting is intended to reformulate the problem as a semidefinite programming problem.

We employ masks $\{M_i\}_{i=1,\dots,N_m}$ to implement the multiple structured illumination. Each mask, denoted as $M_i \in \mathbb{R}^{N\times N}$ for $i = 1,\dots,N_m$, is a diagonal matrix. Specifically, the first mask, $M_1 = I$, is chosen as the identity matrix. The diagonal entries of the other masks are randomly set to 0 or 1 to create random diffraction patterns. By substituting the discrete source function

$$\boldsymbol{f} := (f(t_0),\dots,f(t_N))^\top$$

with sources using the masks, i.e.,

$${}^i\boldsymbol{f} := M_i\boldsymbol{f}, \quad i = 1,\dots,N_m,$$

we obtain additional discrete solutions $\{{}^iu_0^n\}_{n=0,\dots,N}^{i=1,\dots,N_m}$ and the noisy data $\{{}^i\hat{u}_0^{n_\omega,\epsilon}\}_{n_\omega=1,\dots,N_\omega}^{i=1,\dots,N_m}$ in the frequency domain. These can be utilized to derive more phaseless Fourier modes $\{|{}^i\hat{f}^\epsilon(\omega_{n_\omega})|\}_{n_\omega=1,\dots,N_\omega}^{i=1,\dots,N_m}$. This procedure can be summarized as follows:

$$\boxed{{}^i\boldsymbol{f}} \xrightarrow[\text{FDM}]{(5.1)} \boxed{{}^iu_0^n} \xrightarrow[\text{noisy data}]{(5.2)} \boxed{{}^iu_0^{n,\epsilon}} \longrightarrow \boxed{{}^i\hat{u}_0^{n_\omega,\epsilon}} \xrightarrow[\text{Spectral cutoff}]{(5.3)} \boxed{|{}^i\hat{f}^\epsilon(\omega_{n_\omega})|}.$$

We refer to [3, 16] for further details on the implementation of the PhaseLift method. Additionally, we suggest consulting [4] for access to the specific code used in the PhaseLift algorithm.

5.3. Numerical examples. In this subsection, we present two illustrative examples to demonstrate the effectiveness of the numerical approach. In these numerical examples, the values for the final time T, as well as the numbers of subintervals in time N and space M, are set as follows: $T = 4\pi, N = 100, M = 128$. Furthermore, to approximate the variance of the solution in (5.3), we take a total of P sample paths. The specific choice for the parameter P will be detailed in each individual numerical example.

Example 1. Consider a smooth function $f(t) = \sin(t)\exp(-t/6)$.

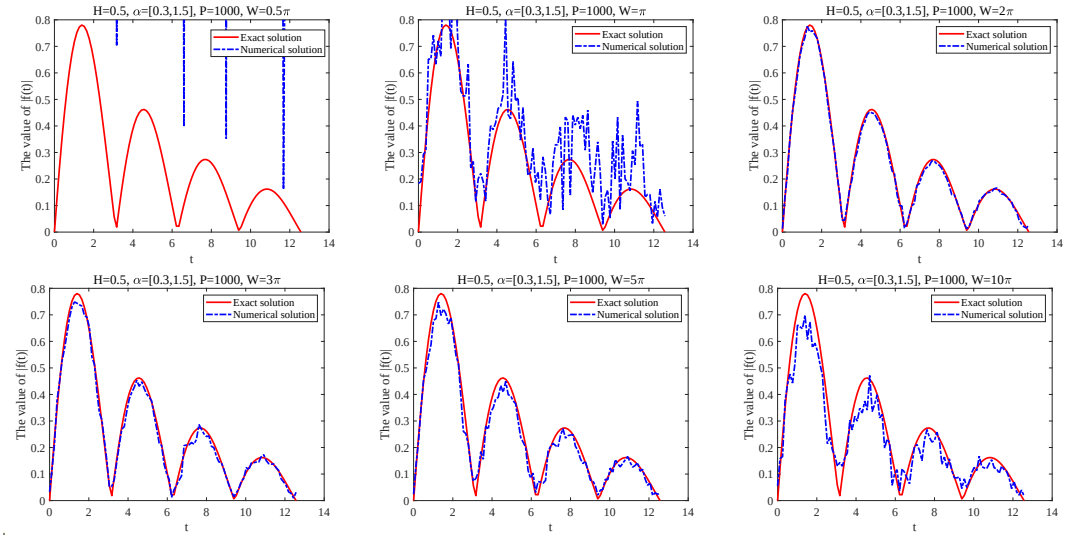

Figure 2. *Example 1: Reconstruction of $|f(t)|$ with varying values of $W = 0.5\pi,\ \pi,\ 2\pi,\ 3\pi,\ 5\pi,\ 10\pi$, while keeping other parameters fixed ($H = 0.5,\ \boldsymbol{\alpha} = [0.3, 1.5],\ P = 1000,\ N_m = 60,\ \epsilon = 5\%$).*

In Example 1, multiple tests are conducted to illustrate the impact of various parameters on the numerical implementation. These parameters include the regularization parameter W, the quantity of masks N_m, the number of sample paths P, the Hurst parameter H, the order $\boldsymbol{\alpha}$ of the fractional derivative, and the noise level ϵ.

Figure 2 presents the numerical results for the reconstruction of $|f(t)|$ in Example 1 with different spectral cut-off regularization parameters, specifically $W = 0.5\pi, \pi, 2\pi, 3\pi, 5\pi, 10\pi$. The remaining parameters are held constant: $H = 0.5$, $\boldsymbol{\alpha} = [0.3, 1.5]$, $P = 1000$, $N_m = 60$, and $\epsilon = 5\%$. The results demonstrate that the reconstruction quality undergoes deterioration when W is excessively small, indicating insufficient information acquisition in the frequency domain, or when it is excessively large, leading to instability in the inverse problem. Therefore, it is crucial to select appropriate regularization parameters, tailored to the specific case at hand. To guide this selection process, we refer to the values of $R(\omega)$ plotted in Figure 1 in relation to ω. For $\boldsymbol{\alpha} = [0.2, 0.3]$, Figure 1 shows that $R(\omega)$ decays slowly as ω increases, suggesting that a relatively larger regularization parameter W should be chosen to ensure that the truncation error remains sufficiently small. Conversely, for cases $\boldsymbol{\alpha} = [0.3, 1.5]$ and $\boldsymbol{\alpha} = [1.1, 1.5]$, $R(\omega)$ decays much faster, indicating that a smaller W would be adequate. In forthcoming numerical tests, we adopt $W = 10\pi$ for cases with $\boldsymbol{\alpha} = [0.2, 0.3]$ and select $W = 3\pi$ for those with $\boldsymbol{\alpha} = [0.3, 1.5]$ or $[1.1, 1.5]$.

In Figure 3, we investigate the impact of varying the number of masks, denoted as N_m, in Example 1, while maintaining constant values for $W = 3\pi$, $H = 0.5$, $\boldsymbol{\alpha} = [0.3, 1.5]$, $P = 1000$, and $\epsilon = 5\%$. The findings illustrate the necessity of employing a sufficient number of masks to ensure the acquisition of an adequate quantity of diffraction patterns, thereby enabling an accurate reconstruction. Based on the numerical results depicted in Figure 3, for subsequent numerical tests, we always choose $N_m = 60$.

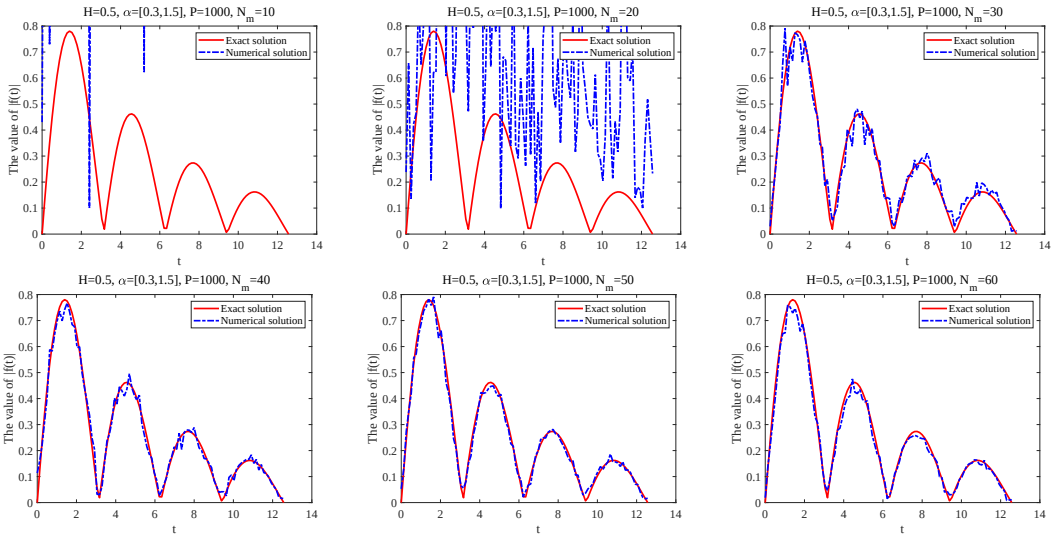

Figure 3. *Example 1: Reconstruction of $|f(t)|$ with varying values of $N_m = 10:10:60$, while keeping other parameters fixed ($H = 0.5$, $\boldsymbol{\alpha} = [0.3, 1.5]$, $P = 1000$, $W = 3\pi$, $\epsilon = 5\%$).*

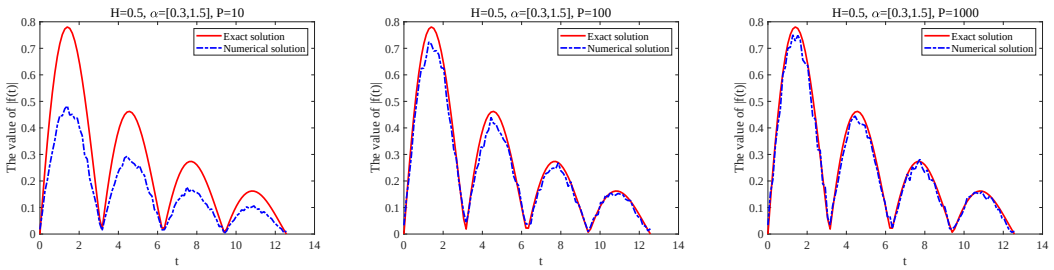

Figure 4. *Example 1: Reconstruction of $|f(t)|$ with varying values of $P = 10, 100, 1000$, while keeping other parameters fixed ($H = 0.5$, $\boldsymbol{\alpha} = [0.3, 1.5]$, $W = 3\pi$, $N_m = 60$, $\epsilon = 5\%$).*

Figure 4 displays the numerical results of the reconstruction of $|f(t)|$ in Example 1 under different sample path quantities, denoted as $P = 10, 100, 1000$, while maintaining fixed values for $H = 0.5$, $\boldsymbol{\alpha} = [0.3, 1.5]$, $W = 3\pi$, $N_m = 60$, and $\epsilon = 5\%$. The observations indicate that the quality of reconstruction improves as more sample paths are employed to approximate the solution's variance, aligning with the principles of the law of large numbers. Notably, the numerical results suggest that a satisfactory level of reconstruction is already achieved with the choice of $P = 1000$. Consequently, we use $P = 1000$ as the fixed sample path quantity in subsequent experiments.

Figures 5–7 depict the influence of parameters $H = 0.3, 0.5, 0.7$, $\boldsymbol{\alpha} = [0.2, 0.3]$, $[0.3, 1.5]$, $[1.1, 1.5]$, and $\epsilon = 1\%, 5\%, 10\%$, while keeping W, N_m, and P fixed, as previously specified. Upon examination of the subfigures within each row, it becomes evident that, for fixed values of H and $\boldsymbol{\alpha}$, the results exhibit relatively higher quality when the noise level, ϵ, is reduced. Likewise, within each column of these figures, when both H and ϵ are held constants, decreasing the value of $\boldsymbol{\alpha}$ leads to improved results. These trends align with the prior theoretical

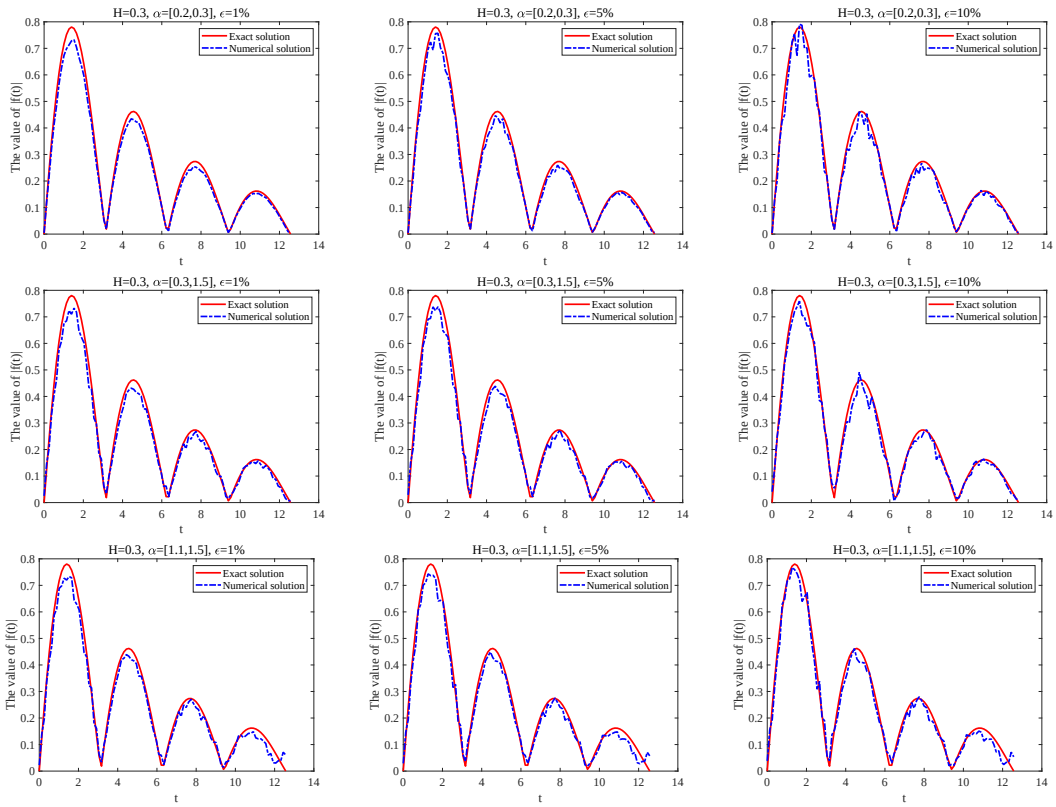

Figure 5. *Example 1: Reconstruction of $|f(t)|$ with different levels of noise: (left) $\epsilon = 1\%$, (middle) $\epsilon = 5\%$, and (right) $\epsilon = 10\%$, while varying the values of $\boldsymbol{\alpha}$ under the constant Hurst parameter $H = 0.3$.*

analysis. Furthermore, through a comparative assessment of the results at corresponding positions in Figures 5–7, it appears that the outcomes are less sensitive to variations in the Hurst index H when compared to alterations in other parameters.

Example 2. Consider a discontinuous function

$$f(t) = \begin{cases} 0, & t \in [0, 4\pi/5), \\ 2, & t \in [4\pi/5, 8\pi/5), \\ 0.5, & t \in [8\pi/5, 12\pi/5), \\ 1.5, & t \in [12\pi/5, 16\pi/5), \\ 0, & t \in [16\pi/5, 4\pi). \end{cases}$$

This example was also examined in [16], and it is challenging to reconstruct due to the presence of infinitely many Fourier modes, with the corresponding Fourier coefficients decaying slowly. In this example, we will not provide a detailed investigation of the impact of various parameters on the reconstruction, as the findings are similar to those in Example 1. Instead, we present the results using carefully chosen representative parameter values. In Figure 8, numerical results showing the reconstruction of $|f(t)|$ in Example 2 are presented. The parameters used for this representation include $H = 0.7$, $\boldsymbol{\alpha} = [1.1, 1.5]$, $W = 3\pi$, $N_m = 60$,

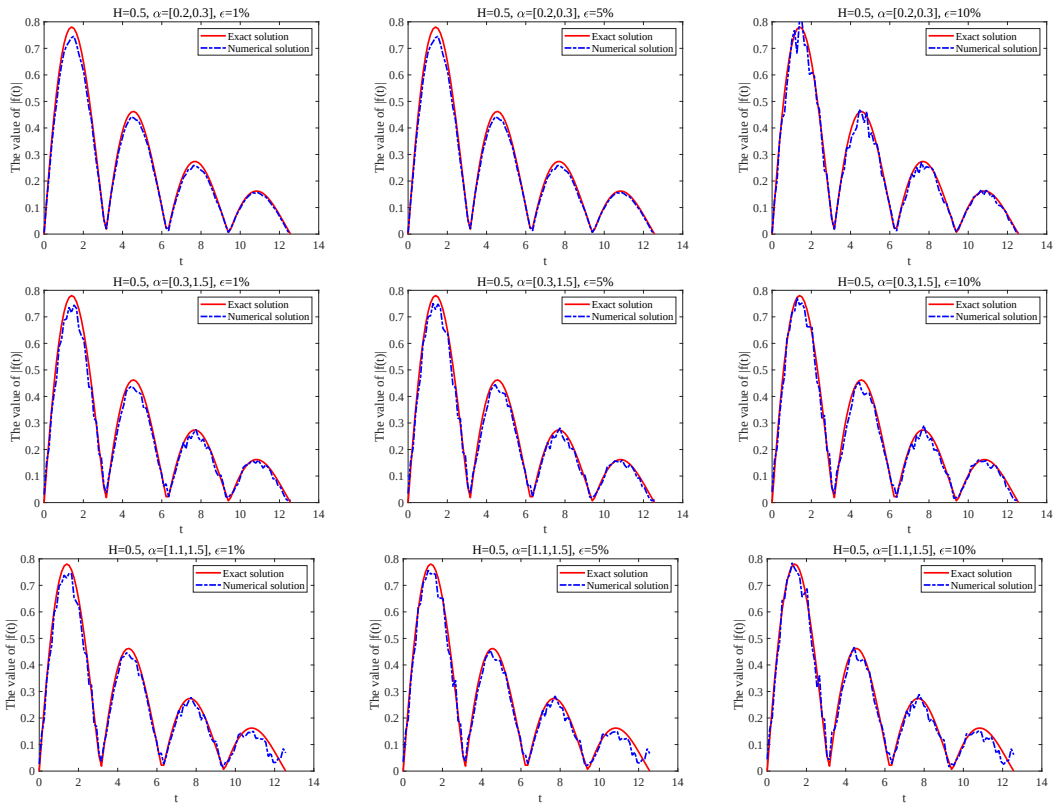

Figure 6. *Example* 1*: Reconstruction of* $|f(t)|$ *with different levels of noise: (left)* $\epsilon = 1\%$*, (middle)* $\epsilon = 5\%$*, and (right)* $\epsilon = 10\%$*, while varying the values* $\boldsymbol{\alpha}$ *under the constant Hurst parameter* $H = 0.5$*.*

$P = 1000$, and varying noise levels $\epsilon = 1\%, 5\%, 10\%$. Despite the emergence of the Gibbs phenomenon, a common occurrence when recovering discontinuous functions through Fourier transform based methods, the proposed algorithm demonstrates strong performance in handling the discontinuous case.

6. Conclusion. This paper addresses both the direct and inverse source problems associated with the stochastic multiterm time-fractional diffusion-wave equation. Regarding the direct random source problem, the well-posedness is obtained by demonstrating the well-posedness of its counterpart in the frequency domain. Furthermore, an analysis is conducted concerning the uniqueness and instability of the inverse random source problem in the frequency domain. To reconstruct the source function in the time domain, the PhaseLift method, combined with the spectral cut-off regularization technique, is utilized for numerical implementation. The numerical results validate the effectiveness of the proposed method.

This work expands upon existing results related to inverse random source problems for stochastic time-fractional differential equations, addressing more general cases. Specifically, it contains (1) subdiffusion cases with $\alpha_i \in (0, 1)$, superdiffusion cases with $\alpha_i \in (1, 2)$, and the classical diffusion case $\alpha_i = 1$, and (2) spatial random noise, which can be represented by fBm noise with $H \in (0, 1)$ as opposed to the traditional Gaussian white noise with $H = \frac{1}{2}$. Several

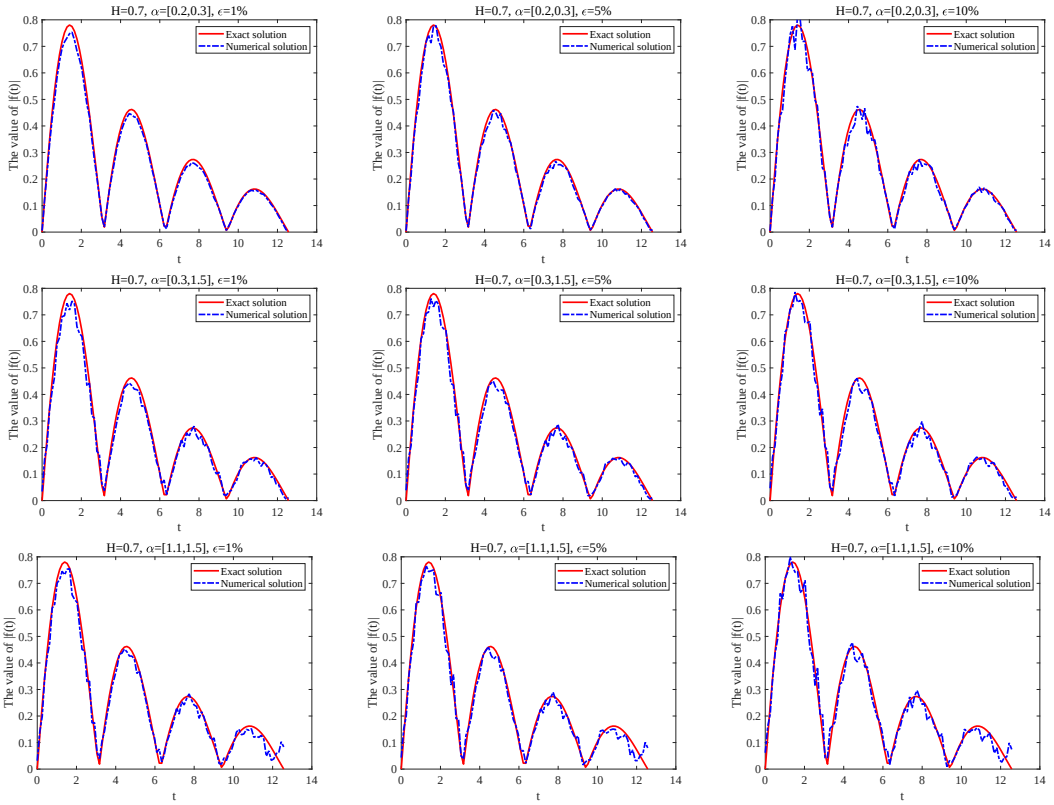

Figure 7. *Example 1: Reconstruction of $|f(t)|$ with different levels of noise: (left) $\epsilon = 1\%$, (middle) $\epsilon = 5\%$, and (right) $\epsilon = 10\%$, while varying the values $\boldsymbol{\alpha}$ under the constant Hurst parameter $H = 0.7$.*

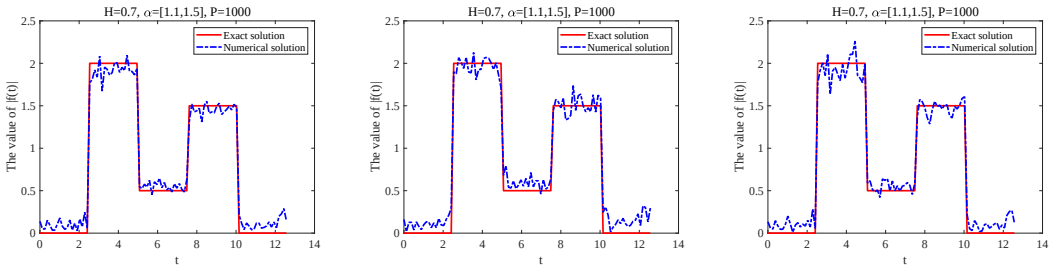

Figure 8. *Example 2: Reconstruction of $|f(t)|$ with different combinations: (left) $\epsilon = 1\%$, (middle) $\epsilon = 5\%$, and (right) $\epsilon = 10\%$, under the constant Hurst parameter $H = 0.7$ and $\boldsymbol{\alpha} = [1.1, 1.5]$.*

challenges remain unresolved, including inverse random source problems in higher dimensions, and inverse random potential problems for time-dependent stochastic partial differential equations, among others. In higher-dimensional cases, establishing a modified isometry formula similar to the one in Lemma 3.4 becomes significantly more challenging. For inverse problems involving random potentials, additional linearization techniques will need to be applied to address these nonlinear inverse problems effectively. We anticipate providing updates on our progress in addressing these challenges in future publications.

REFERENCES

[1] K. Abuasbeh, R. Shafqat, A. U. K. Niazi, and M. Awadalla, *Nonlocal fuzzy fractional stochastic evolution equations with fractional Brownian motion of order* (1,2), AIMS Math., 7 (2022), pp. 19344–19358, https://doi.org/10.3934/math.20221062.

[2] R. A. Adams, *Sobolev Spaces*, Academic Press, New York, 1975.

[3] E. J. Candes, Y. C. Eldar, T. Strohmer, and V. Voroninski, *Phase retrieval via matrix completion*, SIAM Rev., 57 (2015), pp. 225–251, https://doi.org/10.1137/151005099.

[4] R. Chandra, T. Goldstein, and C. Studer, *PhasePack: A phase retrieval library*, in Proceedings of the 13th International Conference on Sampling Theory and Applications (SampTA), 2019, pp. 1–5.

[5] A. V. Chechkin, R. Gorenflo, and I. M. Sokolov, *Retarding subdiffusion and accelerating superdiffusion governed by distributed-order fractional diffusion equations*, Phys. Rev. E, 66 (2002), 046129, https://doi.org/10.1103/PhysRevE.66.046129.

[6] C. F. M. Coimbra, *Mechanics with variable-order differential operators*, Ann. Phys., 12 (2003), pp. 692–703, https://doi.org/10.1002/andp.200351511-1203.

[7] V. Daftardar-Gejji and S. Bhalekar, *Boundary value problems for multi-term fractional differential equations*, J. Math. Anal. Appl., 345 (2008), pp. 754–765, https://doi.org/10.1016/j.jmaa.2008.04.065.

[8] S. Das, *Functional Fractional Calculus*, Springer, New York, 2011.

[9] A. Dasgupta, *Fractional Brownian Motion: Its Properties and Applications to Stochastic Integration*, University of North Carolina at Chapel Hill, 1997.

[10] O. Drosinou, C. V. Nikolopoulos, A. Matzavinos, and N. I. Kavallaris, *A stochastic parabolic model of MEMS driven by fractional Brownian motion*, J. Math. Biol., 86 (2023), pp. 1416–1432, https://doi.org/10.1007/s00285-023-01897-6.

[11] X. Feng, P. Li, and X. Wang, *An inverse random source problem for the time fractional diffusion equation driven by a fractional Brownian motion*, Inverse Problems, 36 (2020), 045008, https://doi.org/10.1088/1361-6420/ab6503.

[12] S. Fu and Z. Zhang, *Application of the generalized multiscale finite element method in an inverse random source problem*, J. Comput. Phys., 429 (2020), 110032, https://doi.org/10.1016/j.jcp.2020.110032.

[13] S. Ghasemalipour and B. Fathi-Vajargah, *Fuzzy simulation of European option pricing using mixed fractional Brownian motion*, Soft Comput., 23 (2019), pp. 13205–13213, https://doi.org/10.1007/s00500-019-03862-2.

[14] M. Giona, S. Cerbelli, and H. E. Roman, *Fractional diffusion equation and relaxation in complex viscoelastic materials*, Phys. A, 191 (1992), pp. 449–453, https://doi.org/10.1016/0378-4371(92)90566-9.

[15] T. Goldstein and C. Studer, *PhaseMax: Convex phase retrieval via basis pursuit*, IEEE Trans. Inform. Theory, 64 (2018), pp. 2675–2689, https://doi.org/10.1109/TIT.2018.2800768.

[16] Y. Gong, P. Li, X. Wang, and X. Xu, *Numerical solution of an inverse random source problem for the time fractional diffusion equation via phaselift*, Inverse Problems, 37 (2021), 045001, https://doi.org/10.1088/1361-6420/abe6f0.

[17] M. El Hassouni, A. Tafraouti, H. Toumi, E. Lespessailles, and R. Jennane, *Fractional Brownian motion and Rao geodesic distance for bone X-ray image characterization*, IEEE J. Biomed. Health. Inform., 21 (2017), pp. 1347–1359, https://doi.org/10.1109/JBHI.2016.2619420.

[18] D. Harker and J. Kasper, *Phases of Fourier coefficients directly from crystal diffraction data*, Acta Cryst., 1 (1948), pp. 70–75, https://doi.org/10.1107/S0365110X4800020X.

[19] H. Jiang, F. Liu, I. Turner, and K. Burrage, *Analytical solutions for the multi-term time-space Caputo-Riesz fractional advention-diffusion equations on a finite domain*, J. Math. Anal. Appl., 389 (2012), pp. 1117–1127, https://doi.org/10.1016/j.jmaa.2011.12.055.

[20] S. Jiang and Y. Wu, *An inverse space-dependent source problem for a multi-term time fractional diffusion equation*, J. Math. Phys., 61 (2020), 121502, https://doi.org/10.1063/5.0007738.

[21] L. A. Knowles, R. A. Bennett, and C. Harig, *Vertical displacements of the Amazon Basin from GRACE and GPS*, JGR Solid Earth, 125 (2020), pp. 1–24, https://doi.org/10.1029/2019JB018105.

[22] M. Lassas, Z. Li, and Z. Zhang, *Well-posedness of the stochastic time-fractional diffusion and wave equations and inverse random source problems*, Inverse Problems, 39 (2023), 084001, https://doi.org/10.1088/1361-6420/acdab9.

[23] Y. Li, L. Sun, Z. Zhang, and T. Wei, *Identification of the time-dependent source term in a multi-term time-fractional diffusion equation*, Numer. Algorithms, 82 (2019), pp. 1279–1301, https://doi.org/10.1007/s11075-019-00654-5.

[24] Z. Li, Y. Liu, and M. Yamamoto, *Initial-boundary value problems for multi-term time-fractional diffusion equations with positive constant coefficients*, Appl. Math. Comput., 257 (2015), pp. 381–397, https://doi.org/10.1016/j.amc.2014.11.073.

[25] C. Liu, J. Wen, and Z. Zhang, *Reconstruction of the time-dependent source term in a stochastic fractional diffusion equation*, Inverse Probl. Imaging, 14 (2020), pp. 1001–1024, https://doi.org/10.3934/ipi.2020053.

[26] Y. Liu, *Strong maximum principle for multi-term time-fractional diffusion equations and its application to an inverse source problem*, Comput. Math. Appl., 73 (2017), pp. 96–108, https://doi.org/10.1016/j.camwa.2016.10.021.

[27] C. Lu, W. Qin, C. Huang, Y. Zhang, and T. K. Ealotswe, *Impact of fractional probability distributions on statistics of hydraulic conductivity, dynamics of groundwater flow and solute transport at a low-permeability site*, Hydrol. Process., 34 (2020), pp. 4112–4127, https://doi.org/10.1002/hyp.13869.

[28] R. Metzler and J. Klafter, *The random walk's guide to anomalous diffusion: A fractional dynamics approach*, Phys. Rep., 339 (2000), pp. 1–77, https://doi.org/10.1016/S0370-1573(00)00070-3.

[29] E. Di Nezza, G. Palatucci, and E. Valdinoci, *Hitchhiker's guide to the fractional Sobolev spaces*, Bull. Sci. Math., 136 (2012), pp. 521–573, https://doi.org/10.1016/j.bulsci.2011.12.004.

[30] P. Niu, T. Helin, and Z. Zhang, *An inverse random source problem in a stochastic fractional diffusion equation*, Inverse Problems, 36 (2020), 045002, https://doi.org/10.1088/1361-6420/ab532c.

[31] D. Nualart, *The Malliavin Calculus and Related Topics*, 2nd ed., Probab. Appl., Springer-Verlag, Berlin, 2006.

[32] A. L. Patterson, *Ambiguities in the X-ray analysis of crystal structures*, Phys. Rev., 65 (1944), pp. 195–201, https://doi.org/10.1103/PhysRev.65.195.

[33] A. Runacher, M. J. Kazemzadeh-Parsi, D. Di Lorenzo, V. Champaney, N. Hascoet, A. Ammar, and F. Chinesta, *Describing and modeling rough composites surfaces by using topological data analysis and fractional Brownian motion*, Polymers, 15 (2023), 1449, https://doi.org/10.3390/polym15061449.

[34] K. Sakamoto and M. Yamamoto, *Initial value/boundary value problems for fractional diffusion-wave equations and applications to some inverse problems*, J. Math. Anal. Appl., 382 (2011), pp. 426–447, https://doi.org/10.1016/j.jmaa.2011.04.058.

[35] G. Samorodnitsky and M. S. Taqqu, *Stable Non-Gaussian Random Processes: Stochastic Models with Infinite Variance,* Chapman & Hall, New York, 1994.

[36] W. R. Schneider and W. Wyss, *Fractional diffusion and wave equations*, J. Math. Phys., 30 (1989), pp. 134–144, https://doi.org/10.1063/1.528578.

[37] Z. Sun and G. Gao, *Fractional Differential Equations: Finite Difference Methods*, Walter de Gruyter, Berlin, 2020.

[38] I. Waldspurger, A. d'Aspremont, and S. Mallat, *Phase recovery, MaxCut and complex semidefinite programming*, Math. Program., 149 (2015), pp. 47–81, https://doi.org/10.1007/s10107-013-0738-9.